FACT-mediated maintenance of chromatin integrity during transcription is essential for viability of mammalian stem cells

Imon Goswami[1]*, Poorva Sandlesh[1, *, #], Aimee Stablewski[2], Ilya Toshkov[3], Mikhail Magnitov[4], Jianmin Wang[5], Katerina Gurova[1]

[1] Department of Cell Stress Biology, Roswell Park Comprehensive Cancer Center, Buffalo, NY, USA;

[2] Transgenic Shared Facility, Roswell Park Comprehensive Cancer Center, Buffalo, NY, USA

[3] Buffalo BioLabs, Buffalo, NY, USA

[4] Institute of Gene Biology Russian Academy of Sciences, 119334 Moscow, Russia

[5] Department of Biostatistics and Bioinformatics, Roswell Park Comprehensive Cancer Center, Buffalo, NY, USA

* These two authors contributed equally to the work. *Corresponding authors*: Katerina Gurova, Department of Cell Stress Biology, Roswell Park Comprehensive Cancer Center, Elm and Carlton Streets, Buffalo, NY, USA, 14263. Tel: 716-845-4760, email: katerina.gurova@roswellpark.org, Jianmin Wang, Department of Biostatistics and Bioinformatics, Roswell Park Comprehensive Cancer Center, Buffalo, NY, USA, 14263. Tel: 716-845-1499, email: katerina.gurova@roswellpark.org.

Abstract

Replication and transcription machineries access DNA through unwrapping it from histone core. Preservation of nucleosome structure during replication is a focus of intensive research, while maintenance of nucleosomes during transcription is less studied. Histone chaperone FACT is involved in transcription elongation, although whether it opens nucleosomes for polymerase or protects core histones from loss during passage of polymerase is still unclear.

We used conditional knockout model of *Ssrp1*, subunit of FACT complex, to deplete FACT in mice and monitored consequences of FACT loss to establish the functional relevance of FACT in mammals. FACT loss was lethal for mice at all ages due to failure of hematopoietic and intestinal tissues. In these tissues, only the progenitors completely vanished upon FACT loss, while number of some other cell types were changed up and down. Using isolated stem cells of several tissues we showed that FACT loss was toxic only for stem cells, but not for cells which were differentiated *in vitro*. Chromatin accessibility in stem cells was increased genome wide upon FACT depletion in transcription dependent manner. The most prominent response to the loss of chromatin integrity upon FACT depletion in cells was activation of interferon signaling, followed by accumulation of immune cells in sensitive organs.

Thus, in undifferentiated mammalian cells FACT keeps chromatin stable during transcription elongation and this function of FACT is essential for viability of stem cells.

Introduction

Chromatin organization in cells defines cell identity via providing selective access of transcription machinery to DNA and therefore making existence of cell- and condition- specific transcriptional programs possible. Significant progress was made in the identification of factors involved in the maintenance of chromatin, as well as in the understanding of the structure of these factors and the ways of their interactions with chromatin (*1*). However, this progress was mainly achieved through studies in cell-free conditions or in simplified model organisms, such as yeast or human tumor cells. Role of these factors in the control of gene expression in a cell-specific manner in multicellular organism, including where and when particular factors are active and what are the results of their activity, is still far behind.

One group of such factors, histone chaperone, was long considered as a part of basic replication and transcription machineries responsible for assembly and disassembly of nucleosomes (*2*). Most of them are essential for viability of single cell eukaryote model systems, such as yeast or human tumor cell lines, suggesting that most of them have unique functional niche (*3*). However, studies done in multicellular organisms demonstrated that they are not ubiquitously expressed and that their depletion has different consequences for different cells (*4-7*), suggesting that either their function is not unique, or that control of chromatin integrity may not be required in all cells.

Histone chaperon FACT (FAcilitates Chromatin Transcription) is especially interesting in this regard since in recent years the view of its function as essential transcription elongation factor, providing RNA polymerase access to nucleosomal DNA, was questioned by several mechanistical and structural studies (*8*), (*9*). It was shown that FACT does not bind to nucleosomes fully wrapped with DNA, but it binds to nucleosomes with partially unwrapped DNA (*10-12*).Moreover, it was found that FACT is selectively expressed in multicellular organisms and phenotypes of FACT knockout in C.elegans or D.rerio does not support the proposed function of FACT as an essential transcription elongation factor (*13, 14*). General knockout (KO) of FACT in mice is lethal at blastocyst stage (*15*), when expression of FACT subunits is the highest during embryonic development (*16*). Several types of mammalian normal cells tested in different labs did not show dependence on FACT for growth or viability (*14, 17, 18*), though most of mouse and human tumor cells could not grow and died upon FACT knockdown (*19, 20*). However, what makes tumor cells dependent on FACT is still unclear and this knowledge may be valuable for cancer research.

Absence of FACT expression in most of adult mammalian cells (*16*) suggested that FACT may have cell specific function or that due to specific chromatin state, some but not all cells need FACT. To understand FACT function in multicellular eukaryotes, it would be good to know what types of mammalian cells depend on FACT and what process is disturbed in these cells upon FACT loss. To answer these questions, we generated conditional mouse knockout model which allows histone chaperone FACT can be turned off to observe cell-specific and age-dependent consequences of FACT loss. FACT consists of two subunits, SPT16 (Suppressor of Ty 16) and SSRP1 (Structure Specific Protein 1). Both are stable only being within FACT complex, therefore deletion of one gene leads to the loss of the whole FACT complex (*21*). Mice with insertion of LoxP sites into introns of *Ssrp1* gene were crossed with R26-CreER^{T2} mice to achieve FACT depletion in adult animals using tamoxifen administration (*22*). In this study we report the phenotype of FACT loss in mice at different ages, identify cells dependent on FACT in "FACT-sensitive" organs and propose the reasons of why FACT is essential for some cells, but not others.

Results

1. FACT loss in mice is lethal at all ages

For this study we used mice homozygous for *Ssrp1* mutant allele, *Ssrp1*$^{fl/fl}$ and heterozygous or wild type animals for comparison (*22*). Importantly, it was shown before (*15*) and we confirmed this in this study that mice with one allele of functional *Ssrp1* gene lack any phenotype, thus in many experiments we used them as control. These mice were crossed with Rosa26 CreERT2 (*CreER*$^{T2+/+}$) mice to obtain mice homozygous for both alleles, since presence of one copy of *CreER*^{T2} results in poor or no excision of *Ssrp1* (*22*). To delete *Ssrp1* we treated adult mice with tamoxifen and monitor FACT complex disappearance at protein level. Spleen is the only organ of adult mice where we were able to detect both FACT subunits by immunoblotting before treatment. Thus, we used spleen protein extracts to observe disappearance of FACT complex upon *Ssrp1* KO, induced with tamoxifen. Both SSRP1 and SPT16 proteins were reduced to the minimal level by the 5th day of treatment (Fig.S1). Based on this in the following experiments tamoxifen was administered for 5 days.

By the end of the first week after stop of tamoxifen administration both female and male mice started losing weight and died or were euthanized between 12 and 50 days after stop of treatment. Female died quicker than males (Fig.1A, B). Since Cre was reported to cause DNA damage due to non-specific recombinase activity – we tested effect of tamoxifen administration in mice with two alleles of CreER^{T2} and wild type *Ssrp1* and did not see any toxicity (Fig.S2), suggesting that death of *Ssrp1*$^{fl/fl}$ mice occurred due to the loss of FACT. Older male mice (24-40 weeks at the start of tamoxifen administration) lived longer than younger and female mice, but still died upon FACT loss. Comparison of complete blood counts (CBC) between groups showed significant reduction in the amount of white blood cells, including lymphocytes and granulocytes, but no changes in red blood cells and platelets (Fig.1C). No significant changes in blood biochemistry were found in these mice (data not shown). Before death mice showed sign of dehydration, some animals developed skin lesions similar to atopic dermatitis (Fig.1D). Attempt to provide extra-fluid to animals through subcutaneous saline injections (1-2 ml/day) did not rescue mice (Fig.S3). Thus, we established that although FACT is present in limited number of cells in several organs of adult mice (*16*), it is essential for viability of mice of all ages. For the following experiments we used mice between 10 and 15 weeks of age.

2. Several tissues are sensitive to FACT depletion

For this study we excluded skin from the analyses, since skin lesions were observed in far from all mice and they were not the reason of lethality upon FACT depletion. Gross pathology examination revealed complete loss of adipose tissue (Fig. 1E, F) and accumulation of liquid in large intestine (Fig.1E). Weight of major parenchymal organs was not significantly changed, excepts spleen, which was smaller in tamoxifen treated groups (Fig. S4). Ovaries were also significantly reduced in tamoxifen-treated mice (Fig.S5A), but these changes were observed in mice with wild type *Ssrp1* gene and reported in literature as direct effect of tamoxifen treatment (*23*). At the same time another organ with high expression of FACT, testis (*16*), were not reduced upon tamoxifen treatment (Fig.S4 and S5B).

Histological changes were found in organs known to express FACT (*16*). Reduced cellularity was observed in bone marrow and spleen. In spleen atrophic changes were seen in red pulp (Fig.2A), areas where FACT is present in basal conditions (*16*). High levels of FACT are also present in cells at the bottom of crypts of small and large intestine (*16*). *Ssrp1* KO resulted in thinning of colon villi and some number of degenerative crypts (Fig. 2A, B). We did not find any changes in "high" FACT organ, testes (Fig.S5B). However, when we tested expression of FACT in testes after tamoxifen administration, we did not see any reduction (Fig. S6A), suggesting that recombination did not occur in testes most probably due to the limited access of tamoxifen through blood-testis barrier (*24*).

Among FACT-negative organs tamoxifen administration causes histological changes only in liver. There was loss of glycogen granules in hepatocytes, some of hepatocytes were enlarged, some were undergoing mitosis, what is not typical for adult liver. Infiltration with lymphoid cells was seen in some areas (Fig.2C).

Altogether these finding may be interpreted as suppression of hematopoiesis, suppression of renewal capacity of intestine leading to atrophic changes, what may explain dehydration, since large intestine is the major organ of water absorption. Changes in liver are most probably secondary in response to weight loss and dehydration. Loss of adipose tissues explains weight loss and may be either primary (death of adipocytes) or secondary (loss of fat from cells due to malnutrition and dehydration) to FACT loss.

3. FACT loss impairs proliferation and induces death of cells in several organs

To reveal the reason of failure of FACT sensitive organs we compared the level of proliferation and cell death in major parenchymal organs between vehicle and tamoxifen-treated mice using

EdU assay and staining for cleaved caspase 3. Three days after stop of tamoxifen treatment EdU was administered to mice for 1 hour before collection of organs. Number of EdU positive cells was significantly reduced in spleen (Fig.3A,C), while in opposite, normally absent EdU positive cells appeared in liver upon FACT knockout in line with observed mitotic cells in H&E stained liver sections (Fig.2C and S6B). Changes in small and large intestine were moderate, with some sections almost without changes in the number of EdU positive cells and some showing reduced frequency of replicating cells at lower portion and spread of replicating cells towards upper portion of crypts. This pattern was noticed in small intestine (Fig.3B,C). In line with histological analysis there were no change in EdU staining of testis between vehicle and tamoxifen treated male mice (Fig.S6A).

In spleen, intestine and colon we observed slight increase in the number of cells stained positive for cleaved caspase 3, however, they were not concentrated in any specific cellular zones of these organs (Fig.3D and S7).

Thus, we observed so far that FACT depletion led to the reduction in number of cells in hematological organs and intestine. Loss of cells is predominantly due to the reduced proliferation of cells in these organs and slight increase in cell death. However, hepatocytes in liver start proliferating upon *Ssrp1* KO. Thus, general impairment of DNA replication or mitosis, processes in which FACT function was reported (*25-28*), (*29*) cannot explain toxicity of *Ssrp1* KO.

4. FACT depletion is accompanied by loss of stem cells in bone marrow and intestine

To find cells, which viability depends on FACT *in vivo*, we treated mice with tamoxifen or vehicle for 5 days and 24 hours after the end of treatment we collected samples of the most FACT-dependent tissues, bone marrow and intestine (including portion of small and large intestine), dissociated them to single cell suspension and analyzed gene expression in individual cells by single cell RNA sequencing (scRNA-seq). Quality control confirmed integrity and viability of >90% of cells of bone marrow and > 75% of cells of intestine for both vehicle and tamoxifen treated samples. There were comparable number of cells sequenced (~8,000 – 10,000 per sample), close number of reads generated (~20,000 – 27,000) and number of genes quantified (~1000 per cell) (Fig.S8A).

First, we noticed that UMAPs plots from vehicle and tamoxifen treated samples of bone marrow and intestine have significant overlap suggesting that in general tissue architecture was well preserved in both organs (Fig.S8B and C). At the same time there were clear changes in

abundance of several cell clusters both up and down. We knew that in sensitive cells FACT depletion leads to the problems with replication (Fig.3A-D and ref. (*26*)), however here using classification of cells based on cell cycle markers (see Material and Methods) we did not observe any changes in cell cycle distribution between vehicle and tamoxifen treated cells (Fig.S9A, B).

In bone marrow there were at least two clusters with visibly increased number of cells (Fig.4A, red ovals) and one completely new small cluster (Fig.4A red arrow) upon FACT depletion. Three clusters completely disappeared (Fig.4A, blue oval). While clusters with increased number of cells (red ovals on Fig.4A) were located separately from each other, disappeared clusters were all located together (blue oval on Fig.4A), suggesting similarity between these cells. To identify bone marrow cells, we used Immunological Genome Project (ImmGen) database (*30*). Clusters with visibly increased number of cells consisted of progenitors of B cells and T cells, while disappeared clusters consisted of stem cells (Fig.4B). Quantitative evaluation of the number of each cell type before and after treatment confirmed increase of pro-B and B cells, T cells and several other mature cell types (Fig.4C, D). Interestingly, cluster of B cells (Fig.4B, grey dashed oval) in fact consisted of two clusters (Fig.4A), upper yellow and lower purple, and these two clusters underwent opposite changes (yellow went up and purple – down). This may suggest that not number of specific B cells, but their transcriptional program was changed upon FACT loss. To define this change, we run gene set enrichment analysis (GSEA) on genes differentiating yellow and purple clusters (Fig.4E and Table S1). Genes common between purple and yellow clusters belong to the list of genes 'upregulated in B cells versus neutrophils and DC' with the highest FDR q-value (2.5e-100). Genes specific for yellow cluster were enriched within 'adaptive immune system' (q = 2e-13), 'cytokine signaling' (q = 1e-8) and 'interferon response pathway' (q = 4.7e-6). Genes specific for purple cluster were enriched within 'splicing' (q = 1e-16), 'metabolism of RNA' (q = 1.5e-16), and 'ribosomal biogenesis' (q = 1.5e-8) categories. Thus, these data suggest that FACT depletion in B cells resulted in inhibition of expression of genes involved in RNA and protein synthesis, and induction of genes of IFN signaling.

Surprisingly and contrary to visual impression quantitation of cell types showed slight increase, instead of decrease in the number of stem cells (Fig.4C, D). The reason for this discrepancy we found in the fact that UMAP of bone marrow control sample contained two separate regions with predominantly stem cells (Fig.4F): one central, isolated from all other hematopoietic cells and another one, connecting monocytes and granulocytes. Only stem cells of central isolated clusters (Fig.4A, blue oval and 4F) disappeared, while other clusters of stem cells located between leukocytes stayed intact and the only noticeable change was emergence of additional "stroke" of

cells shown with red arrow on Fig.4A. To find out the difference between these subpopulations of bone marrow stem cells we used ImmGen datasets specific for bone marrow stem cells. We identified 11 sets of cells with stem cell markers (Fig.4G, H). However, some subsets contain very few cells (≤5) in any of samples (vehicle and tamoxifen), so we excluded them from analysis and some apparently discriminate cells which according to the description represent the same subtype of stem cells (e.g. SC.LTHSC and SC.LT34F, or SC.STSL and SC.ST34F), these we combined into one subtype. After this preprocessing, we have found that there is significant redistribution of stem cells between subtypes upon FACT loss (Fig.4G, H). The most dramatic change was observed for long-term hematopoietic stem cells (LT-HSC), cells standing at the start of hematopoietic cell renewal and differentiation. This subpopulation completely disappeared after *Ssrp1* deletion. LT-HSC give rise to short-term HTC (ST-HSC), in our case consisting of SC.STSL and SC.ST34F. Number of these cells was just slightly reduced upon FACT loss (27% decrease versus control). Among other stem cells which number was reduced upon FACT loss were multipotent lymphoid progenitors (MLP), megakaryocyte-erythroid progenitors (MEP) and myeloid-dendritic progenitors (MDP), though some cell types were substantially increased, among which granulocytic-myeloid progenitors (GMP) and T, B and NK cells at different stages of maturation. Thus, we observed that the most sensitive to FACT depletion in bone marrow was the earliest hematopoietic progenitors, LT-HSC.

General architecture of intestine cell clusters was also well preserved (Fig.5A and Fig.S8C). Three neighboring clusters were completely lost (Fig.5A, clusters # 5, 9 and 12) and several increased or emerged de novo (# 1-3, 10, 12, 13, 15 and 19). For recognition of intestinal cells, we used data published by Gao et all (*31*) and Haber et all (*32*). All clusters were ascribed to certain intestinal cell types, except cluster #2, which was not identified (Table S2). Marker genes of the most prominently lost cluster # 5 was enriched within 'large intestine Lgr5 positive stem cells'. Cells of this cluster also have high expression *Gkn3*, marker of small intestine stem cells defined by Haber (*32*). Genes of disappeared cluster #9 were enriched within two gene sets: 'small intestine enterocyte progenitors subtype 1 and 2' (q = 1.7e-6) and 'large intestine enterocytes progenitors' (q = 4.66e-6). This was very similar to disappeared cluster #12 which genes are enriched within the same lists but with much lower FDR (q-values 2.1e-32 and 7.28e-17 respectively, Fig.5A). Three downregulated clusters (# 5, 9, 12) form one axis suggesting that cells of these clusters are in transition from intestinal stem cells (cluster #5) through cells with a less number of emerging markers of enterocyte progenitors (cluster #9) to cells with highly significant presence of markers of enterocyte progenitors (cluster #12).

Surprisingly, major clusters of cells which number was increased upon FACT loss (# 6, 10, 13) were classified quite similarly to disappeared clusters. The lowest FDRs were 'small intestine enterocyte progenitors subtype 2' according to Gao (*31*) (# 6 q = 1.91 e-34, #10 q = 5.1 e-11, # 13 q = 3.88 e-30). They were all located close to each other and just below cluster of disappeared cells (Fig.5A and S8C) what suggested that cells of disappeared clusters (# 9 and 12) and emerged clusters (# 6, 10, 13) may be the same cells (enterocyte progenitors) but which transcriptional program was changed upon FACT loss. Thus, if we consider all these cells as enterocyte progenitors and run GSEA on genes differing clusters 6 + 10 +13 versus 9 +12, then we can conclude that depletion of FACT in enterocyte progenitors results in downregulation of genes enriched among 'eukaryotic translation' (q = 3.4e-166), 'ribosome' (q = 1.7e-160) and multiple similar pathways, and upregulation of genes of interferon response (q = 2.7e-4) (Table S3). This was surprisingly similar to what we saw in bone marrow B cells.

There were little changes in the number of cells in clusters 0 and 4, composed of distal enterocytes according to Haber or large intestinal enterocytes according to Gao. Quantitation revealed mild changes in the number of some other cell types, including slight increase in the number of Goblet cells and their progenitors and Paneth cells (clusters #14 and #21).Cluster #21 emerged only upon FACT loss but was enriched in markers of Paneth cells, suggesting that there was changes in expression of a group of genes in Paneth cells. Looking for differentially expressed genes between these two clusters showed that group of small ribosomal proteins are expressed at higher level in cluster #14 and markers of Paneth cells are elevated in newly emerged cluster #21, suggesting that cells of cluster #21 may be more mature than cells in cluster #14. Another cluster, which number was increased is #15 and cells composing this cluster have gene expression signature of large intestine immune cells (FDR q-value = 9.93 e-65) as well as Dclk1 positive cells, marker of intestinal tuft cells.

In general changes in intestinal cell composition were similar to those seen in bone marrow: disappearance of intestinal stem cells and some progenitors and increase in the number of more mature cell types, such as small enterocyte progenitors or Goblet and Tufts cells. Thus, scRNA-seq analyses confirmed our previous observations that the most undifferentiated stem cells are the most sensitive to FACT loss, while differentiated cells are not. Cell in between stem and fully differentiated most probably respond to FACT loss with reduction in active RNA and protein synthesis (characteristic of proliferating cells) and induction of IFN response.

5. Stem cells of several organs are unable to expand *in vitro* in the absence of FACT

To confirm that stem cells are dependent on FACT for viability and growth, we compared colony forming ability of stem cells of FACT-sensitive organs. We plated cells isolated from bone marrow, small intestine and colon in special media supporting growth of stem cells and treated them with 4-hydroxytamoxifen (4-OHT, active metabolite of tamoxifen) to induce *Ssrp1* deletion *in vitro*. We also added to these experiment mesenchymal stem cells (MSC) from adipose tissue to figure out whether loss of adipose tissue is primary or secondary effect of *Ssrp1* KO. While growth of skin fibroblasts from tails of the same mice was not affected by deletion of *Ssrp1* (*20*), growth of all stem cells was significantly reduced. No colonies were formed from bone marrow of *Ssrp1*$^{fl/fl}$*; CreER*^{T2} mice in the present of 4-OHT, while 4-OHT did not interfere with the growth of bone marrow cells with genotypes not resulting in bi-allelic *Ssrp1* deletions (Fig.6A, B). No organoids were formed from small intestine or colon stem cells from *Ssrp1*$^{fl/fl}$*; CreER*^{T2} mice upon 4-OHT administration, although growth of intestinal and colon cells not forming organoids was reduced, but not stopped (Fig.6C, D). MSC were growing but at a slower pace than vehicle treated cells and their number was reduced due to the increase in apoptosis upon FACT depletion (Fig.6E, H).

Next, we tested if cells lose dependence on FACT for viability upon differentiation. For this, we isolated intestinal and adipose stem cells and kept them in conditions which either support their undifferentiated state or induce *in vitro* differentiation using protocols described in literature (*33-35*). In both cases, 4-OHT administration was toxic to undifferentiated cells, while has no effect on differentiated cells. Moreover, in case of MSC we obtained cultures of differentiated adipocytes and osteocytes through providing them with different media as described (*36*). Neither adipocytes nor osteocytes died upon FACT depletion (Fig.6H, I). Thus, we confirmed that only undifferentiated stem cells are dependent on FACT for viability, while differentiated cells are not. In line with this, level of FACT goes down upon differentiation as judged by immunostaining of SSRP1 subunit (Fig. 6G, J).

6. Loss of FACT in stem cells leads to significant changes in chromatin accessibility in transcription dependent manner.

Thus, we found that the earliest progenitors in bone marrow and intestine are highly dependent on FACT and completely disappear upon FACT loss. To understand the reason of stem cell loss upon FACT depletions, we investigated what happens with chromatin structure and transcription in MSC, cells which are sensitive to FACT loss *in vitro*, but do not die upon this. We run bulk RNA-seq and

Assay for Transposase-Accessible Chromatin using sequencing (ATAC-seq) (*37*) with MSC before and after treatment with 4-OHT. As control for both types of assays we used MSC heterozygous for *Ssrp1*^{fl} allele, which did not show any phenotypic changes upon 4-OHT administration (Fig.6E, H).

There was less number of genes which expression was changed in *Ssrp1*$^{fl/+}$ heterozygous cells, while expression of many more genes was changed in homozygous *Ssrp1*$^{fl/fl}$ cells. There was almost no overlap in genes which expression was changed between homo- and heterozygous cells in response to 4-OHT (Fig.S10A), confirming that gene expression changes in *Ssrp1*$^{fl/fl}$ cells are in response to FACT loss and not to 4-OHT administration. Many more genes were upregulated upon FACT loss than downregulated (Fig.7A, B). Changes in gene expression of heterozygous cells were more random (Fig.S10B,C).

Gene ontology (GO) enrichment of upregulated genes showed that the most significant category was interferon response (Fig.7C and Table S4). Downregulated genes did not have dominant category but belongs to 'PI3K-AKT signaling pathway', 'negative regulation of transcription', ECM remodeling, 'negative regulation of cell differentiation' and 'positive regulation of cell proliferation' (Fig.7D and Table S4), many of which reflect the observed phenotypic changes in these cells.

Surprisingly, there was no correlation between changes in gene expression and chromatin accessibility, independently on whether we analyzed reads corresponding to promoter regions, gene bodies or up- and downstream flanking regions (Fig.S11A). Visual investigation of ATAC-seq peaks using genome browser showed that there are regions (broad peaks), mostly at gene bodies, with increased accessibility and narrow peaks, many of which around transcription start site (TSS) with reduced accessibility upon *Ssrp1* KO (Fig. 8A). These opposite changes at TSS and gene body may explain absence of correlation between changes in transcription and chromatin accessibility. However, when we quantitated number of up- and downregulated peaks, associated with different genomic features we found that more peaks were upregulated, than downregulated and upregulated peaks were associated with all genic features (Fig. 8B). Maximal number of downregulated peaks (which was still lower than upregulated) were found in introns and distal intergenic regions, suggesting that these peaks are enhancers. There were very few peaks which emerged *de novo* (17 out of 47620 peaks detected in cells without FACT) or completely disappeared (4 out of 65041 total peaks in cells with FACT) upon FACT depletion, suggestion that FACT loss results in quantitative rather than qualitative changes in chromatin accessibility.

When we built profiles of chromatin accessibility using mean ATAC-seq read density for all mouse genes the most significant difference was reduced height of a peak at TSS in cells without

FACT versus cell with FACT, although slight increase of accessibility at gene body was also noticed (Fig. 8C, red arrow)). To get more detailed view on changes in chromatin accessibility we analyzed separately fragments corresponding to nucleosome-free regions and mononucleosomes as described by Buenrostro (*37*). According to fragment length distribution of our data (Fig. S11B) nucleosome-free reads were ≤87 bp, mononucleosome reads were >167 bp and ≤ 259 bp. Using these set of fragments separately to build profiles of chromatin accessibility around TSS of all known mouse genes +/1 kbp we found that indeed chromatin accessibility was changed significantly in 4-OHT treated homozygous, but much less in heterozygous cells versus control (Fig. S11C). Loss of FACT led to the reduced accessibility at a narrow region around TSS (-200, +70bp for nucleosome-free fragments and -400, +350 for mononucleosome fragments), while increased before and after (Fig.S11C), suggesting that FACT may have different roles in the control of chromatin accessibility during initiation (at TSS) and elongation (gene body) of transcription.

To test whether FACT mediated control of chromatin integrity indeed depends on transcription, we used RNA-seq data to classify genes based on their expression. First, we identified genes which are not expressed in any of the tested conditions, this group consisted of 26,577 genes out of 55,401 total mouse genes analyzed. The remaining 28,824 genes were divided into 4 quantiles based on their average expression in cells with and without FACT. Since distribution of genes based on their expression level is nonlinear with the most of genes expressed at low or very low levels, while very few are expressed at really high level (Fig.S11D), we also analyzed separately a group of genes with the highest level of expression among all (top 1%, 289 genes).

The most dramatic change was seen for the highest expressed genes, for which chromatin accessibility was significantly increased right after TSS (Fig.7D and S12). Difference was gradually reduced from 5' to 3' ends of a gene and disappear right after TES. The difference was also reduced with the reduction of transcription, but still was significant for all transcribed genes independently on whether we quantitated nucleosome-free or mononucleosome fragments (Fig.7E and S12). At TSS itself FACT loss resulted in decrease of chromatin accessibility for all transcription categories, except genes with the highest transcription level where accessibility was not changed for mononucleosomal fragments, but slightly reduced for nucleosome-free (Fig. 7F and S13), suggesting that accessibility here is reduced not due to the assembly of nucleosomes, but probably due to the binding of other proteins.

Although increase in chromatin accessibility at transcribed regions was highly significant, accessibility was not changed at non-transcribed genes, which comprise almost half of all genes. Thus, we were interested how in general chromatin accessibility is changes upon FACT loss in MSC. For this we run simple assay which allows quantitatively assess general chromatin

accessibility in a cell. It is known that access of small molecules binding DNA via minor groove is limited when DNA is wrapped around nucleosome (*38, 39*). Thus, we took advantage of Hoechst 33342, cell permeable minor groove binding molecule, which fluorescence is manyfold increased when it is bound to DNA. We incubated unfixed cells with Hoechst 33342 for 30 minutes and then measured fluorescence per cell using flow cytometry. To avoid potential differences in the amount of DNA per cell due to different phase of cell cycle, we arrested all cells in G1 by serum withdrawal for 48 hrs. As a positive control, we used another small molecule, curaxin CBL0137 which disrupts DNA/histone interactions in cells (*11*). As expected curaxin treatment significantly increases fluorescence of both homo- and heterozygous cells (Fig.S12A). The same effect was caused by treatment of homozygous, but not heterozygous cells, with 4-OHT (Fig.8H and S12B,C).

Thus, we have found that FACT loss resulted in the increase of chromatin accessibility at transcribed regions which degree depends on the level of transcription. Since we was increase in both nucleosome-free and mononucleosomal fragments, this happens most probably due to the opening or partial unwrapping and loss of nucleosomes.

Discussion

Necessity to maintain chromatin organization during replication is recognized as an important control mechanism in eukaryotes. Preservation of chromatin organization during transcription so far got less attention, although data that RNA polymerase “degrades” chromatin has being accumulating (*40-42*). Much more attention was given to the problem of how RNA polymerase access nucleosomal DNA and what factors facilitate this process. During last several years FACT happened to be in transition from the latter, as from the moment of discovery (*43*) it was mainly seen as a factor facilitating transcription through chromatin, to the former, as the data were accumulating questioning FACT role as a factor opening nucleosomes to RNA polymerase (reviewed in (*8, 44*)).

These data may be summarized as follows: (i) there was no evidence that removal of FACT from eukaryotic cells results in inhibition of transcription, while there were data that FACT depletion in several model systems resulted in no change or even increase in absolute level of transcription (*19, 20*); (ii) there was no strong data showing that FACT can bind and destabilize nucleosome with fully wrapped DNA, while there were data showing that FACT binds all nucleosome components and nucleosomes not fully wrapped with DNA (rev. in (*44*) and the most recent study (*10*)); (iii) there were observations that removal of FACT from cells results not in accumulation, but in loss of histones from chromatin (*45-47*). These sets of data led to the emergence of a new

model for FACT role in transcription: nucleosomes are opened by transcription machinery or associated factors without help of FACT, but FACT binds components of nucleosomes, histone dimers and tetramers, as well as possibly DNA to preserve nucleosomes at their position during transcription. This model explained also initially puzzling observation that while , FACT enrichment at mammalian genes is highly proportional to the level of transcription, transcription of genes bound by FACT is not inhibited by FACT removal (*17, 20, 48*). While profile of FACT enrichment at genes fitted very well with originally proposed function of FACT as a factor facilitating RNA polymerase passage through chromatin, increase in the rate of transcription upon FACT loss did not within this model. However, these observation are explained by the new model: the higher the transcription (i.e. the more frequent is the passage of RNA polymerase through a region), the more frequently nucleosomes are disturbed, the more chances are for FACT to bind. Then, as it was shown before, binding of DNA back to histone core displaces FACT due to higher affinity of histones to DNA, than histones to FACT (*49*). Therefore, genes with lower transcription, i.e. with less frequent passage of RNA polymerase, accumulate less FACT. At the same time if FACT loss is accompanied by the loss of nucleosomes from the transcribed region, then we might expect increase in transcription at this region.

Here we tested and confirmed this proposed model in mammalian system. We also demonstrated that function of FACT as a major factor responsible for maintenance of chromatin during transcription is essential for viability of a small fraction of cell in adult mice. However, these cells are vital for viability of adult mice, since KO of *Ssrp1* was lethal for mice at all tested ages. Together with previously published data that general KO of *Ssrp1* was lethal at 3.5 dpc (*15*), our new data allow to conclude that *Ssrp1* is essential gene in mammals due to be essential for survival of stem cells.

Tissues the most sensitive to FACT loss were hematopoietic and intestinal, both known to be dependent on constant replenishing of cells from tissue-specific stem cells. The earliest progenitors in both systems were completely lost upon KO *Ssrp1.* Stem cells in other tissues are probably also sensitive for FACT loss, as we saw in non-essential adipose tissue. Skin abnormalities seen in mice upon FACT depletion suggest that skin stem cells are also abolished upon FACT loss, but this proposition requires additional observation. For testing of the role of FACT in viability of other tissues, tissue-specific KO of *Ssrp1* is needed to prevent death of animals from failure of bone marrow and intestine.

At the same time FACT is not essential for many types of adult cells, as we saw before (*19, 20*). Here we established that many cell types, mostly differentiated but also some progenitors, were increased in number upon FACT loss. Most probably this is due to the compensatory redistribution of populations of cells independent on FACT. However, to establish this, time dependent monitoring of organ cell composition upon *Ssrp1* KO is needed. At the same time, abundance of cell types which number was increased, even among stem and progenitor cells, suggest that multiple adult cells do not need FACT for survival.

Importantly, there were many proliferating cells among FACT independent types. We also did not see changes in cell cycle distribution upon FACT loss via scRNA-seq, suggesting that stem cells disappear not due to the problems with replication or mitosis, processes where FACT functioning was observed (*25, 29*). Thus, an important question is what makes these cells sensitive to FACT loss. We partially responded to this question by showing that loss of FACT results in significant increase in chromatin accessibility. Previously we observed that in differentiated fibroblasts, which express low level of FACT and is not sensitive to *Ssrp1* KO, removal of FACT does not lead to the loss of nucleosomes, while in oncogene-transformed cells it does (*20*). So, we can propose that there is specific state of nucleosomes in some stem or transformed cells, which makes them dependent on FACT for stability, and these state of nucleosomes makes these cells dependent on FACT for viability.

There is clear difference between sensitivity of chromatin to FACT loss depending on transcription, i.e. the higher is the transcription the stronger is increase in chromatin accessibility upon FACT removal at gene bodies. Unexpectedly, we found that there is decrease in chromatin accessibility at narrow regions around TSS, which is less dependent on transcription. The mechanism of this is obscure and maybe proposed as elevated deposition of histones lost from transcribed regions.

There is also not so clear relationship between changes in transcription and chromatin accessibility upon FACT loss since there was no correlation changes in RNA-seq and ATAC-seq data. This absence of correlation may be explained by the fact that chromatin accessibility is changed oppsotely at gene bodies than at TSS. Gene transcription is regulated by accessibility of TSS, while loss of nucleosomes at gene bodies most probably leads to cryptic initiation and emergence short living non-functional transcripts, which we did not accurately measure with bulk RNA-seq of poly-A-enriched RNA. Methods assessing nascent RNA synthesis is needed to look for correlation between chromatin accessibility and transcription.

An interesting observation which may led light on physiological consequences of chromatin destabilization is increase in number of T and B cells in bone marrow and immune cells in intestine. If in bone marrow, increase in B cells may be due to shift in differentiation, the number of T cells in bone marrow and immune cells in intestine may only be increased due to migration these cells. This accumulation may be related to the fact that the most upregulated pathway in response to *Ssrp1* KO in all cell systems which we looked here, was interferon response. We also observed activation of interferon type I pathway in response to a different way of chromatin destabilization, treatment of mice with small molecule curaxin CBL0137 disrupting histone/DNA binging (*11*). Interferons are well-established factors attracting immune cells to the sites of viral invasion and inflammation (*50*). The mechanism of interferon activation upon chromatin destabilization is not fully established, but in case of curaxin this was dsRNA accumulating in cells due to the transcription of pericentromeric repeats (*51*). The same mechanism may be involved in case of FACT depletion, although several other may not be excluded, such as emergence of cryptic initiation with synthesis of uncapped RNA activating RIG/MAVS5 pathway or binding of nuclear cGAS to DNA losing nucleosomes.

Thus, we established that in adult mammals FACT performs unique function in earliest progenitor stem cells of several organs. Long-term hematopoietic stem cells of bone marrow as well as Lgr5+ cells of intestine cannot survive in the absence of FACT. FACT in these cells is critical for the maintenance of chromatin during transcription. Loss of FACT results in the loss of nucleosomes at transcribed genes and elevated transcription. The most significantly upregulated pathway in response to the increase of chromatin accessibility is interferon signaling, which is most probably responsible for the accumulation of immune cells in sensitive organs in response to FACT loss.

Materials and Methods

Reagents

Reagents	Source	Catalogue #	Application
Chemicals and Kits			
DMEM-High Glucose with Pyruvate And L-Glutamine	Corning	MT 10-013-CV	Cell culture
0.05% Trypsin EDTA	Corning	MT 25-052-Cl	Cell culture
10,000U Pen Strep	Corning	MT 30-002-CI	Cell culture
FBS, USDA, Regular, Heat Inactivated	Corning	MT 35-011-CV	Cell culture
α-MEM	Stem Cell Technologies	36450	Cell culture
Advanced DMEM/F-12	Gibco	12634010	Intestinal organoid culture
GlutaMAX™ Supplement	Gibco	35050061	Intestinal organoid culture
IMDM-Iscove's Media with LGlutamine	Gibco	MT 10-016-CV	Bone marrow colony forming assay
MethoCult™ GF M3434	Gibco	03434	Bone marrow colony forming assay
KnockOut DMEM	Gibco	10829018	mESC cell culture
Complete Protease Inhibitors – Cocktail, Tablets	Roche	04693132001	Preparation of protein extract
Laemmli sample buffer	BioRad	1610737	Sample preparation for immunoblotting
Quick Start ™ Bradford 1x dye reagent	BioRad	500-0204	Measurement of protein concentrations
4–20% gradient precast gels	BioRad	4561094	PAGE
PVDF membranes	BioRad	1620177	Immunoblotting
Western Lightning Plus-ECL	PerkinElmer	NEL104001EA	Enhanced luminescence
Hoechst 33342	Invitrogen	H3570	Staining of DNA
4-hydroxytamoxifen	Millipore Sigma Aldrich	H7904-5MG	Induction of Ssrp1 deletion (in vitro)
Tamoxifen	Millipore Sigma Aldrich	T5648-1G	Induction of Ssrp1 deletion (in vivo)
Caspase-3 substrate (Ac-DEVD-AMC)	Enzo Life Sciences	ALX-260-031-M001	Apoptosis assay

Click-iT™ EdU Alexa Fluor™ 488/594 imaging kit	Thermo Fischer Scientific	C10337	Proliferation assay, EdU staining of tissue sections
Alizarine Red S	Millipore Sigma Aldrich	A5533-25G	Staining of differentiated osteocytes
Oil Red O	Millipore Sigma Aldrich	O0625-25G	Staining of differentiated adipocytes
Methylene blue	Millipore Sigma Aldrich	M4159	Measuring cell viability
Resazurin sodium salt	Millipore Sigma Aldrich	R7017-1G	Measuring viability of intestinal organoids
Collagenase A	Millipore Sigma Aldrich	10103578001	Isolation of fibroblasts and mesenchymal stem cells
Dexamethasone	Millipore Sigma Aldrich	D4902	Differentiation of mASC
isobutylmethylxanthine (IBMX)	Millipore Sigma Aldrich	I5879-100MG	Differentiation of mASC
Insulin	Gibco	12585014	Differentiation of mASC
β-glycerophosphate	Millipore Sigma Aldrich	50020-100G	Differentiation of mASC
L-ascorbic acid	Millipore Sigma Aldrich	A92902-25G	Differentiation of mASC
Gentamycin	Gibco	15710064	Culturing of intestinal organoids
Murine recombinant EGF	PeproTech	315-09	Culturing of intestinal organoids
Murine recombinant Noggin	PeproTech	250-38	Culturing of intestinal organoids
Human recombinant R-Spondin 1	PeproTech	120-38	Culturing of intestinal organoids
Matrigel	BD Biosciences	356237	Culturing of intestinal organoids
Valproic acid sodium salt	Millipore Sigma Aldrich	P4543-10G	Culturing of intestinal organoids
Stemolecule CHIR99021	Reprocell	04-0004	Culturing of intestinal organoids
Nextera kit	Illumina	FC-121-1030	ATAC-seq
NEBNext High-Fidelity 2X PCR Master Mix	New England Biolabs	M0541	ATAC-seq
MinElute PCR Purification kit	Qiagen	28004	ATAC-seq
mRNA HyperPrep kit	KAPA BIOSYSTEMS	KK8580	RNA-seq
Antibodies			

SSRP1 mouse monoclonal 10D1	Biolegend	609702	Immunoblotting: 1:3000 Immunohistochemistry: 1:200
SPT16 monoclonal mouse 8D2	Biolegend	607002	Immunoblotting: 1:1000
beta-actin mouse monoclonal (HRP conjugated)	Millipore Sigma Aldrich	A3854	Immunoblotting 1:20,000
Mouse Lgr5/GPR49 Antibody	R&D Systems	MAB8240-SP	Immunohistochemistry: 1:200
Cleaved caspase 3	Thermo Fisher Scientific	**700182**	Immunohistochemistry: 1:200
m-IgGκ BP-HRP	Santa Cruz Biotechnology	sc-516102	Immunoblotting: 1:4000
Secondary anti-mouse Alexa Fluor® (488 and 594)	Life Technologies	A-11062 and 11001	Immunohistochemistry: 1:500

10 mg/ml tamoxifen solution was prepared by dissolving 100 mg tamoxifen powder in 100 ul proof ethanol and the mixture was slowly dissolved in 9.8 ml sterile corn oil at 37 ºC overnight. 5mM stock solution of 4-hydroxytamoxifen (4OHT) was prepared by dissolving 5 mg 4-hydroxytamoxifen powder in 2.5 ml proof ethanol. Final working solution used was 2uM.

Alizarin red S was prepared by dissolving 2 g powder in 100 ml distilled water and mixed well. The pH of the solution was adjusted to 4.1-4.3 with 10% ammonium hydroxide. The solution was stored at 4ºC away from light. Oil red O stock solution was prepared by dissolving 0.7 g powder in 200 ml isopropanol, stirred overnight, filtered with 0.2 um filter and stored at 4ºC away from light. Working solution was prepared fresh by diluting 6 parts oil red O stock and 4 parts distilled water, mixed and allowed to sit at room temperature for 20 minutes and filtered through 0.2 um filter.

2.5mM (36X) Resazurin was prepared by dissolving 0.629g resazurin sodium salt powder (Milipore Sigma Aldrich) in DPBS and sterilized by filtering through 0.22 um filter. The solution was stored in 50 ml aliquots at -20ºC away from light for long term storage. The 36X solution is diluted to 6X solution for use which can be stored at 4ºC away from light for upto 3 months. The 6X solution is used at a final concentration of 70 uM.

Animal experiments

Animal breeding and treatment: all animal breeding, maintenance and experiments were conducted in accordance with the Institute Animal Care and Use Committee (IACUC) at Roswell Park Comprehensive Cancer Center. Mice were maintained in the Laboratory Animal Shared Resource with controlled air, light, and temperature conditions, and fed ad libitum with 5% fat chow with free access to water.

Conditional FACT Knockout (cKO) mouse model with the following genotypes were generated as previously described (Sandlesh et al., 2018): *SSRP1*$^{fl/fl}$ *;CreERT2*$^{+/+}$ (KO mice), *SSRP1*$^{+/+}$

;CreERT2$^{-/-}$ (wild type), *SSRP1*$^{+/+}$ *;CreERT2*$^{+/+}$, *SSRP1*$^{fl/fl}$ *;CreERT2*$^{-/-}$, *SSRP1*$^{fl/fl}$ *;CreERT2*$^{-/-}$, *SSRP1*$^{fl/+}$ *;CreERT2*$^{+/-}$ (controls).

Mice of different ages were treated with 1mg of tamoxifen in 100 ul solution or 100 ul of vehicle by daily IP injection for 5 days. In some experiments, mice received daily subcutaneous injection of 1 ml of 0.9% saline. Mice weights and cage site observations were recorded daily. Animals were euthanized upon losing 20% of body weight by CO_2 asphyxiation and cervical dislocation following IACUC protocols. All cells, tissues and organs were harvested under sterile conditions.

Mouse tissue collection and staining: Mouse tissues were harvested and preserved in 10% buffered formalin. Sections of paraffin-embedded tissues were cut at 5µm and staining with H&E, anti-SSRP1 and cleaved caspase 3 antibodies were performed at the Immunohistochemistry Lab of the RPCI Pathology Resource Network using standard techniques. All slides were scanned using Aperio system (Aperio Technologies, Inc). Images were made using Image Scope software (Aperio Technologies, Inc).

For EdU staining, three days after end of treatment, mice were injected with 50mg/kg EdU (Thermo Fisher Scientific) one hour before organs were harvested. Tissue sections were processed using Click-iT EdU Alexa 488 Fluor Imaging kit (Thermo Fisher Scientific) and counterstained with DAPI (Life Technologies) following manufacturer's instructions. Samples were examined using a Zeiss AxioImager A1 microscope equipped an epifluorescent light source. Images were captured with an AxioCam MRc digital camera and processed with a Zeiss Axio Imager Z1 microscope software (Carl Zeiss, Germany).

MRI Imaging: 2 mice of each gender and genotype were used. MR images were taken on day 0 (before), and days 6, day 8 and day 10 after the start of treatment with tamoxifen or vehicle.

MR images were acquired on a 4.7 Tesla, preclinical MRI scanner using the ParaVision 3.0.2 platform (Bruker Biospin, Billerica MA). A 72 mm (I.D.) quadrature RF coil was used to capture volumetric data from the entire mouse body. Two NMR tubes filled with 1mM and 3 mM CuSO4 in 1% agarose were included in each session for signal normalization. Following scout scans, a three-dimensional, fast spin echo scan was acquired with the following parameters: TE/TR = 6.2/100 ms, echo train length = 4, averages =4, FOV = 113x55x35 mm, matrix=256x128x128, zero-filled to achieve an isotopic voxel size of 273 microns. Image signal intensities were normalized by a three-point correction curve using the two phantoms and background noise, and the whole-body volume was segmented and calculated using a region-growing tool in commercially-available software (Analyze 7.0, AnalyzeDirect, Overland Park KS). Adipose tissue was segmented from lean tissue using a fixed intensity threshold derived from the average threshold of all datasets, as reported by the Ostu method, and confirmed by visual inspection. Percent adipose tissue volume was calculated by ratio of voxels segmented as adipose tissue divided by total body voxels.

Complete Blood Counts (CBC) and Blood Biochemistry: 50ul of blood for CBC was collected from saphenous vein as described (*52*) before treatment (to determine baseline CBC) as well as on day 12 and 15 after start of treatment. CBC measurements were made at Buffalo Biolabs LLC.

For blood biochemistry, blood was collected from deeply anesthetized mice via cardiac puncture. Blood was collected into serum separator tubes (Sarstedt), allowed to clot at room temperature for at least 15 minutes, then centrifuged at 10,000 RCF for 10 minutes. Serum was collected into a separate tube and run through the IDEXX Catalyst DX Chemistry Analyzer (Idexx Laboratories, serial # 89-37997-02). Chem 17 clips (Idexx Laboratories) were used for our sample analysis.

Cells

Mesenchymal stem cells (MSCs) were harvested from adipose tissue of 8-10 week old mice. Tissue was minced and digested with 2mg/ml collagenase A in PBS and 2% BSA at 37 ºC with shaking for 30 minutes. The digested tissue was filtered through 40 um filter and centrifuged at 300g for 5 minutes. Cells were resuspended in DMEM with 10% FBS and 1% penicillin-streptomycin and plated.

MSC differentiation into adipocytes and osteocytes. MSCs were plated on 60 mm plates and allowed to be 80% confluent. Differentiation into adipocytes was induced by supplementing media with 250 nM dexamethasone, 66 nM insulin and 0.5 mM isobutylmethylxanthine (IBMX) for 21 days. Differentiation into osteocytes was induced by supplementing media with 0.1uM dexamethasone, 10mM β-glycerophosphate and 50uM L-ascorbic acid for 14 days. Media with differentiation factors were changed every 2-3 days. Differentiation into adipocytes and osteocytes was tested by staining with Oil Red O and Alizarin Red (see below). After differentiation cells were treated with 2 uM 4OHT for 5 days and viability of undifferentiated MSCs and differentiated adipocytes/osteocytes was tested.

For adipocyte or osteocyte staining, media was removed, cells were washed with PBS and fixed with 10% neutral buffered formalin for 30 minutes with gentle shaking at room temperature. Formalin was removed, cells were washed twice with distilled water and 60% isopropanol was added for 5 minutes. Then for working solution of oil red O (for adipocyte staining) or Alizarin red S (for osteocyte staining) were added and plates were incubated at room temperature protected from light for 20 (oil red O) or 45 minutes (Alizarin red S). After that stains were removed, wells were washed twice with distilled water, covered with water and images were taken under light microscope.

Intestinal stem cells were collected by procedure previously described (*53*). Briefly, 15 cm of intestine was harvested from mice and placed in cold PBS. The intestine was cut open longitudinally and flushed with cold PBS. The tissue was cut into 5 mm pieces in 2 mM EDTA in PBS with 50 ug/ml gentamycin and incubated at 4 ºC with gentle shaking for 30 minutes. The EDTA-PBS was discarded, tissue was resuspended in cold PBS and vigorously shaken to dislodge the crypts. The suspension was allowed to settle by gravity for 5 minutes and the supernatant containing villus fraction was discarded. The tissue was resuspended in cold PBS and shaken vigorously again to enrich the supernatant with crypt fraction. The crypt fraction was filtered through 70 um filter and centrifuged at 200g for 3 minutes at 4 ºC. The pellet was resuspended in crypt culture medium: Advanced DMEM:F12 with 2% FBS, 50 ug/ml gentamycin, L-2 mM glutamine, 50 ng/ml EGF, 500 ng/ml R-spondin 1, 100 ng/ml Noggin, 1 mM valproic acid sodium salt and 3 uM CHIR99021. Crypts were counted using hemocytometer and 500 crypts were mixed with 50 ul Matrigel at 4ºCand pipetted in the center of 24 well plates prewarmed to

37ºC. The domes were allowed to set for 10 minutes at 37 ºC in incubator and 500 ul of crypt culture medium was gently added to each well. Organoids were allowed to form over 7-10 days and media was changed every 2-3 days. Crypts were passaged following protocol of Sato et al., (*53*). Briefly, 2mM EDTA-PBS was added to each well and pipetted to break the Matrigel dome and release crypts. The suspension is centrifuged at 200g at 4ºC for 3 minutes. The pellet is washed with PBS, centrifuged and resuspended in 50ul Matrigel. The suspension is pipetted at the center of 24 well plates prewarmed to 37ºC, allowed to set at 37ºC for 10 minutes and 500 ul of crypt culture media is added to each well.

After two passages, the organoids were treated with 2 uM 4OHT for 5 days. On day 6, the organoids were split into new wells and allowed to grow for 5-7 days. Ability to form colony was assessed by counting number of organoids in untreated and treated wells and normalizing to number of colonies formed from untreated wells.

To differentiate organoids, intestinal stem cells isolated as described above were cultured in medium without R-spondin 1 for 2.5 days as described by Lindeboom (*33*). Undifferentiated organoids were maintained in media containing R-spondin 1. The differentiated and undifferentiated organoids were treated with 2 uM 4OHT for 5 days and viability was tested at the end of treatment.

At the end of differentiation, organoids were fixed in 4% paraformaldehyde (PFA) for 30 minutes which partly dissolves the Matrigel. The organoids were collected in a tube, centrifuged at 2000 rpm for 5 minutes at room temperature. The PFA was discarded and pellets were washed with PBS. Organoids were permeabilized by incubating with 0.1% Triton X-100 in 3% BSA+PBS at room temperature on rotator and then blocked with 0.05% Triton X-100 and 1% BSA+PBS for one hour on rotator. Staining was done via incubation of organoids with the following primary antibodies: SSRP1 (1:200), Lgr5 (1:200) on rotator at 4ºC overnight. The organoids were washed with blocking solution and incubated with secondary antibodies: anti-rat Alexa Fluor 488 (1:500) against Lgr5 and anti-mouse Alexa Fluor 594 (1:500) against SSRP1, for 1 hour at room temperature on rotator, protected from light. The organoids were washed with blocking solution, then with PBS and stained with Hoechst (1:2000 in PBS) for 30 minutes on rotator at room temperature away from light. They were washed with PBS and resuspended in PBS and plated on 96 well plates. Images were taken on Zeiss Axio Imager Z1 microscope (Carl Zeiss, Germany).

For **bone marrow** colony forming assay femur and tibia of mice were excised from hindlimbs by removing connective tissue and cleaned with 70% ethanol. The bones crushed in a sterile mortar and pestle with PBS to generate a single cell suspension which was filtered through 70 um cell strainer. The process was repeated once more till bones appear white indicating al marrow has been removed. Cells were counted using a hemocytometer and a suspension containing 4.5 x 10^5 nucleated cells/ml was prepared. Complete IMDM media was prepared by adding 20 ml IMDM to 80 ml MethoCult M3231. 2uM working concentration of 4OHT or DMSO (control) were added to 4.1 ml of complete IMDM by inverting the tube and vortexing for 5 seconds twice. The tube was then placed in a refrigerator for 5 minutes to allow bubbles to escape. 400 ⌠l of 4.5 x 10^5 cells/ml bone marrow cell suspension was added to each tube of medium and 4OHT or control mix. Tubes were mixed gently by inverting tube two times and vortexing three times for 8 seconds each on

maximum speed. Tubes were placed in refrigerator for 5 minutes to allow bubbles to escape. 1 ml cell+medium+4OHT/control mixture is plated on 35 mm dishes using primed 5 ml syringe with a 19 G needle. Final cell density per 35 mm plate was 40,000. Plates were incubated at 37ºC and colonies were allowed to form on methylcellulose in presence or absence of 4OHT for 7 days.

Viability assays

For methylene blue assaymedium was removed from plates and 0.5% solution of methylene blue in 50% methanol was added. Cell plates were incubated with methylene blue for 15 minutes at room temperature with gentle shaking. Then plates were gently washed with distilled water and allowed to dry. 1% solution of sodium dodecyl sulfate (SDS) in PBS was used to extract dye by shaking at room temperature for 30 minutes and absorbance was read at 595 nm.

For measuring viability of intestinal organoids resorufin assay was used. Intestinal organoids were cultured, differentiated or maintained in undifferentiated state and treated with or without 2 uM 4OHT for 5 days in 96 well plates in 100 ul media. At the end of treatment, 20 ul 6X resorufin solution was added to each well at final concentration of 70 uM and plates were incubated at 37ºC for 6 hours. Absorbance was read at 570 nm.

EdU staining

Cells were treated with 2 uM 4OHT for 5 days and EdU staining was performed using the Click-iT® Plus EdU Imaging Kit (Invitrogen) according to manufacturer's instructions. Cells were treated for 1 hour at 37 ºC incubator with 20 uM of EdU by replacing half of the culture medium with 2X EdU stock solution (40 uM). After incubation medium was removed and cells were fixed with 3.7% PFA in PBS for 15 minutes at room temperature. Then cells were incubated in 3% Bovine Serum Albumin (BSA) in PBS and permeabilized with 0.5% Triton X-100 in PBS for 20 minutes at room temperature. At the end of incubation cells were washed twice with 3% BSA in PBS and Click-iT® Plus reaction cocktail was prepared according to manufacturer's instruction and added to each well for 30 minutes with shaking at room temperature protected from light. After washing with PBS, Hoechst 33342 stain (final concentration 5ug/ml) was added for 30 minutes. Cells were washed with PBS, covered in PBS and images were taken using Zeiss Axio Imager Z1 microscope (Carl Zeiss, Germany).

Immunoblotting

Cells were washed with PBS and lysed on ice with RIPA buffer (150 mM sodium chloride, 1.0% NP-40, 0.5% sodium deoxycholate, 0.1% sodium dodecyl sulfate and 50 mM Tris, pH 8.0) and protease inhibitor (Roche) for 30 minutes. The extracts were centrifuged at 13000 rpm for 15 minutes to remove debris. Protein concentration of supernatants were determined using Quick Start ™ Bradford 1x dye reagent and appropriate volumes containing equal amounts of protein were boiled with Laemmli buffer at 100ºC for 5 minutes. The samples were briefly centrifuged and run on 4–20% gradient precast gels. Following this, the proteins were transferred to PVDF membranes and membraned were blocked with 5% milk at room temperature for one hour with gentle shaking. The membranes were then incubated with primary antibodies: mouse SSRP1,

SPT16 at 4ºC overnight. They were washed and incubated with HRP-conjugated, anti-mouse secondary antibodies for 1 hour at room temperature. For β-actin, membranes were incubated with HRP-conjugated mouse β-actin antibody at room temperature for 1 hour. Membranes were washed incubated for 1 minute with Western Lightning Plus- ECL and images were acquired using BioRad ChemiDoc™ Touch Imaging System.

Caspase assay

Caspase-3 fluorogenic substrate Ac-DEVD-AMC was reconstituted in DMSO to prepare 1mg/ml (1.4 mM) concentration. Cells were lysed with 1X CCLR buffer and amount of protein was estimated using Pierce BCA assay. 100 ug protein was used in 50 ul volume. 50 ul substrate was added (20 mM HEPES, 10% glycerol, 2 mM DTT, 20 uM Ac-DEVD-AMC) for each sample in a 96 well black plate (BD Falcon). Plates were incubated at 37 ºC for 1 hour and fluorescence was measured.

DNA minor groove binding:

Cells were treated with 4OHT for 5 days and then serum starved for 48 hours. For positive control, cells were treated with 1uM of CBL0137 for 30 minutes. 500,000 cells were used for each sample. Cells were washed with PBS and stained with 3 uM Hoechst 33342 in 3% BSA-PBS at 37 ºC for 15 minutes. Flow cytometry was performed to detect fluorescence at XX/ZZ l wavelength using LSRB II (Becton Dickinson). Histograms were constructed using WinList 3D software (Verity Software House).

ATAC-seq

50,000 cells were prepared for ATAC-seq as previously described Buenostro et al (*37*) with slight modifications. Briefly, cells were washed with PBS, lysed and incubated with transposition reaction mixture at 37ºC for 30 minutes. The DNA was purified using Qiagen MinElute PCR Purification Kit and amplified using PCR primer 1 and barcoded primer 2 (1 cycle of 72°C for 5 min, 98°C for 30 sec, 13 cycles of 98°C for 10 sec, 63°C for 30 sec, 72°C for 1 min). Primers were custom synthesized by Integrated DNA Technologies (IDT) and sequences are provided in Buenostro et al. (2013). The PCR products were purified using AmpureXP beads (Beckman Coulter). The resulting libraries are evaluated on High Sensitivity D1000 screentape using a TapeStation 4200 (Agilent Technologies), and quantitated using Kapa Biosystems qPCR quantitation kit for Illumina. They are then pooled, denatured, and diluted to 350pM with 1% PhiX control library added. The resulting pool is then loaded into the appropriate NovaSeq Reagent cartridge and sequenced on a NovaSeq6000 following the manufacturer's recommended protocol (Illumina Inc.).

RNA-seq

The sequencing libraries are prepared with the mRNA HyperPrep kit (KAPA BIOSYSTEMS), from 500ng total RNA following manufacturer's instructions. Briefly, PolyA RNA was purified using mRNA Capture Beads. Purified RNA was fragmented and primed for cDNA synthesis. Fragmented RNA is then reverse transcribed into first strand cDNA using random primers. Second strand cDNA synthesis converts cDNA:RNA hybrid to dscDNA, while marking the 2nd

strand by incorporating dUTP in place of dTTP. Pure Beads were used to separate the ds cDNA from the second strand reaction mix resulting in blunt-ended cDNA. A single 'A' nucleotide is then added to the 3' ends of the blunt fragments. Multiple indexing adapters, containing a single 'T' nucleotide on the 3' end of the adapter, are ligated to the ends of the ds cDNA, preparing them for hybridization onto a flow cell. Adapter ligated libraries are amplified by PCR, purified using Pure Beads, and validated for appropriate size on a 4200 TapeStation D1000 Screentape (Agilent Technologies, Inc.). The DNA libraries are quantitated using KAPA Biosystems qPCR kit, and are pooled together in an equimolar fashion, following experimental design criteria. Each pool is denatured and diluted to 350pM with 1% PhiX control library added. The resulting pool is then loaded into the appropriate NovaSeq Reagent cartridge for 100cycle single-read analysis and sequenced on a NovaSeq6000 following the manufacturer's recommended protocol (Illumina Inc.).

Sample preparation for single cell RNA-sequencing

Bone marrow and intestinal cells of vehicle and tamoxifen treated mice were used for single cell gene expression using 10X Genomics technology. For bone marrow samples, femurs of mice were cleaned with alcohol, washed with ice cold PBS with antibiotic and metaphysis were removed. The marrow was flushed with buffer (2mM EDTA + 0.5% BSA in PBS) using 23G syringe into a 50 ml tube. Cells were gently mixed, filtered through 40 um cell strainer and centrifuged at 300g for 10 minutes. The pellets were resuspended in 0.04% BSA-PBS. Cells were counted using trypan blue and 100,000 cells were used in 1000 cells/ul concentration.

For intestinal samples, small intestine was separated from stomach and caecum and contents were flushed with ice cold PBS with gentamycin using a 20G needle. The intestine was placed in a dish with fresh PBS and cut open longitudinally and walls were washed to remove any residual matter. The intestine was placed in a 50 ml tube with 10 ml ice cold PBS with 10 mM EDTA and incubated at 4ºC with gentle rocking for 30 minutes. The tissue was then transferred to 10 ml fresh, cold PBS and shaken with vigorous bursts to release epithelial cells. The tissue is discarded, and the supernatant is centrifuged at 300 g for 5 minutes at 4ºC. The pellet is washed once with cold PBS, resuspended in PBS with 1 mg/ml collagenase and incubated at 37ºC for 5 minutes. Following this the tube is immediately placed on ice and 5% (v/v) FBS is added. The cell suspension is centrifuged, washed with PBS and filtered through 40 um cell strainer. The pellet is resuspended in 0.04 % BSA-PBS and cells are counted using trypan blue. 100,000 cells were used in 1000 cells/ul concentration.

10X Genomics

Single cell libraries were generated using the 10X Genomics platform. Cell suspensions were first assessed with Trypan Blue using a Countess FL automated cell counter (ThermoFisher), to determine concentration, viability and the absence of clumps and debris that could interfere with single cell capture. Cells were loaded into the Chromium Controller (10X Genomics) where they were partitioned into nanoliter-scale Gel Beads-in-emulsion with a single barcode per cell. Reverse transcription was performed, and the resulting cDNA was amplified. The full-length amplified cDNA was used to generate gene expression libraries by enzymatic fragmentation, end-repair, a-tailing, adapter ligation, and PCR to add Illumina compatible sequencing adapters. The

resulting libraries were evaluated on D1000 screentape using a TapeStation 4200 (Agilent Technologies), and quantitated using Kapa Biosystems qPCR quantitation kit for Illumina. They were then pooled, denatured, and diluted to 300pM with 1% PhiX control library added. The resulting pool was then loaded into the appropriate NovaSeq Reagent cartridge and sequenced on a NovaSeq6000 following the manufacturer's recommended protocol (Illumina Inc.).

Bioinformatic analysis

RNA-seq fastq files were aligned to mouse mm10 genome using STAR (*54*) with GENCODE v25 gene annotation. Differential gene expression was assessed using DESeq2 (*55*) with default parameters. Genes with 1.5 fold change between conditions and FDR <0.05 were considered differentially expressed. GSEA was run using MSigDB website (Broad Institute) and GO enrichment was run using g:Profiler (*56*) (Ensembl v104). Gene lists with FDR q-value $\leq$ 1e-4 were considered significant. For classification of genes based on expression, baseMean column from DESeq2 differential expression result table was used. A list of unexpressed genes was created from genes with baseMean 0. Genes with baseMean > 0 were used for ranking based on expression. For this baseMean values were divided by gene length, ranked and divided into 4 quantiles.

ATAC-seq fastq files were aligned to the same genome using bowtie2 (*57*) with arguments --very-sensitive --no-mixed --no-unal --no-discordant -X 2000. Duplicates were filtered using Picard MarkDuplicates function. Length of fragments corresponding to nucleosome-free, mononucleosome and all nucleosome were established using fragment length distribution plot as described by Buenorstro (*37*) using fragments sizes from all experiments pooled together. Bigwig files with CPM-normalized profiles were obtained using deepTools (*58*), using --maxFragmentlength and --minFragmentlength parameters to account for fragment sizes. Pile-ups were calculated using computeMatrix function in scale-regions or reference-point modes and visualized using plotProfile function from deepTools.

ATAC-seq peaks were called using MACS2 (*59*) with default parameters. ChIPSeeker (*60*) was used to annotate called peaks with genomic features. For the analysis of correlation with RNA-seq, p eaks located +/- 3kb around TSS were classified as promoters, intron and exon peaks were classified as gene bodies, other peaks were classified as downstream or intergenic. Correlation between RNA-seq and ATAC-seq for different genomic regions was calculated using Log2FC data from DESeq2 and ATAC-seq signal density in MACS2 peaks.

For the scRNA-seq Chromium 10x Genomics libraries, the raw sequencing data were processed using Cellranger software (http://software.10xgenomics.com/single-cell/overview/welcome) with mm10 genome and GENCODE annotation. Then the filtered gene-barcode matrices which contain barcodes with the Unique Molecular Identifier (UMI) counts that passed the cell detection algorithm will be used for further analysis. The downstream analyses were performed using Seurat (*61*) single cell data analysis R package. . First, cells were demultiplexed with hashtag oligos (HTOs) and assigned to the corresponding sample., Then the normalized and scaled UMI counts were calculated using the SCTransform method. Additionally, cell cycle scores for S and G2/M phases based on the well-defined gene sets were assigned. Dimension reduction based on Principal component analysis (PCA), UMAP and tSNE were carried out. Data clustering were

identified using the shared nearest neighbor (SNN)-based clustering on the first 30 principal components. SingleR (*62*) package was utilized to identify cell types; for bone marrow samples, the Immgen reference data (*30*) are used and for intestine samples the markers identified in a single cell studies (*31, 32*) were used. The plots were generated using Seurat and ggplot2 R package.

Statistics

All statistical analysis was performed on GraphPad Prism 8. Data was considered significant if p-value was < 0.05.

References

1. C. Wolberger, How structural biology transformed studies of transcription regulation. *J Biol Chem*, 100741 (2021).
2. C. M. Hammond, C. B. Stromme, H. Huang, D. J. Patel, A. Groth, Histone chaperone networks shaping chromatin function. *Nat Rev Mol Cell Biol* **18**, 141-158 (2017).
3. J. C. Hansen, J. K. Nyborg, K. Luger, L. A. Stargell, Histone chaperones, histone acetylation, and the fluidity of the chromogenome. *J Cell Physiol* **224**, 289-299 (2010).
4. D. Dilg, R. N. Saleh, S. E. Phelps, Y. Rose, L. Dupays, C. Murphy, T. Mohun, R. H. Anderson, P. J. Scambler, A. L. Chapgier, HIRA Is Required for Heart Development and Directly Regulates Tnni2 and Tnnt3. *PLoS One* **11**, e0161096 (2016).
5. J. X. Shi, J. S. Li, R. Hu, X. M. Li, H. Wang, CAF1-knockout mice are more susceptive to lipopolysaccharide-induced acute lung injury. *J Inflamm Res* **9**, 115-121 (2016).
6. S. Messiaen, J. Guiard, C. Aigueperse, I. Fliniaux, S. Tourpin, V. Barroca, I. Allemand, P. Fouchet, G. Livera, M. Vernet, Loss of the histone chaperone ASF1B reduces female reproductive capacity in mice. *Reproduction* **151**, 477-489 (2016).
7. H. P. Voon, J. R. Hughes, C. Rode, I. A. De La Rosa-Velazquez, T. Jenuwein, R. Feil, D. R. Higgs, R. J. Gibbons, ATRX Plays a Key Role in Maintaining Silencing at Interstitial Heterochromatic Loci and Imprinted Genes. *Cell Rep* **11**, 405-418 (2015).
8. T. Formosa, F. Winston, The role of FACT in managing chromatin: disruption, assembly, or repair? *Nucleic Acids Res* **48**, 11929-11941 (2020).
9. K. Zhou, Y. Liu, K. Luger, Histone chaperone FACT FAcilitates Chromatin Transcription: mechanistic and structural insights. *Curr Opin Struct Biol* **65**, 26-32 (2020).
10. Y. Liu, K. Zhou, N. Zhang, H. Wei, Y. Z. Tan, Z. Zhang, B. Carragher, C. S. Potter, S. D'Arcy, K. Luger, FACT caught in the act of manipulating the nucleosome. *Nature* **577**, 426-431 (2020).
11. A. Safina, P. Cheney, M. Pal, L. Brodsky, A. Ivanov, K. Kirsanov, E. Lesovaya, D. Naberezhnov, E. Nesher, I. Koman, D. Wang, J. Wang, M. Yakubovskaya, D. Winkler, K. Gurova, FACT is a sensor of DNA torsional stress in eukaryotic cells. *Nucleic Acids Res* **45**, 1925-1945 (2017).
12. Y. Tsunaka, Y. Fujiwara, T. Oyama, S. Hirose, K. Morikawa, Integrated molecular mechanism directing nucleosome reorganization by human FACT. *Genes Dev* **30**, 673-686 (2016).
13. K. Koltowska, H. Apitz, D. Stamataki, E. M. Hirst, H. Verkade, I. Salecker, E. A. Ober, Ssrp1a controls organogenesis by promoting cell cycle progression and RNA synthesis. *Development* **140**, 1912-1918 (2013).
14. E. Kolundzic, A. Ofenbauer, S. I. Bulut, B. Uyar, G. Baytek, A. Sommermeier, S. Seelk, M. He, A. Hirsekorn, D. Vucicevic, A. Akalin, S. Diecke, S. A. Lacadie, B. Tursun, FACT Sets a Barrier for Cell Fate Reprogramming in Caenorhabditis elegans and Human Cells. *Dev Cell* **46**, 611-626 e612 (2018).
15. S. Cao, H. Bendall, G. G. Hicks, A. Nashabi, H. Sakano, Y. Shinkai, M. Gariglio, E. M. Oltz, H. E. Ruley, The high-mobility-group box protein SSRP1/T160 is essential for cell viability in day 3.5 mouse embryos. *Mol Cell Biol* **23**, 5301-5307 (2003).
16. H. Garcia, D. Fleyshman, K. Kolesnikova, A. Safina, M. Commane, G. Paszkiewicz, A. Omelian, C. Morrison, K. Gurova, Expression of FACT in mammalian tissues suggests its role in maintaining of undifferentiated state of cells. *Oncotarget* **2**, 783-796 (2011).
17. H. Garcia, J. C. Miecznikowski, A. Safina, M. Commane, A. Ruusulehto, S. Kilpinen, R. W. Leach, K. Attwood, Y. Li, S. Degan, A. R. Omilian, O. Guryanova, O. Papantonopoulou, J. Wang, M. Buck, S. Liu, C. Morrison, K. V. Gurova, Facilitates chromatin transcription complex is an "accelerator" of tumor transformation and potential marker and target of aggressive cancers. *Cell Rep* **4**, 159-173 (2013).

18. C. Mylonas, P. Tessarz, Transcriptional repression by FACT is linked to regulation of chromatin accessibility at the promoter of ES cells. *Life Science Alliance* **1**, 1-14 (2018).
19. D. Fleyshman, L. Prendergast, A. Safina, G. Paszkiewicz, M. Commane, K. Morgan, K. Attwood, K. Gurova, Level of FACT defines the transcriptional landscape and aggressive phenotype of breast cancer cells. *Oncotarget* **8**, 20525-20542 (2017).
20. P. Sandlesh, A. Safina, I. Goswami, L. Prendergust, S. Rosario, E. Gomez, J. Wang, K. Gurova, Prevention of chromatin destabilization by FACT is crucial for malignant transformation *iScience*, (2020).
21. A. Safina, H. Garcia, M. Commane, O. Guryanova, S. Degan, K. Kolesnikova, K. V. Gurova, Complex mutual regulation of facilitates chromatin transcription (FACT) subunits on both mRNA and protein levels in human cells. *Cell Cycle* **12**, 2423-2434 (2013).
22. P. Sandlesh, T. Juang, A. Safina, M. J. Higgins, K. V. Gurova, Uncovering the fine print of the CreERT2-LoxP system while generating a conditional knockout mouse model of Ssrp1 gene. *PLoS One* **13**, e0199785 (2018).
23. S. Luo, C. Martel, A. Sourla, S. Gauthier, Y. Merand, A. Belanger, C. Labrie, F. Labrie, Comparative effects of 28-day treatment with the new anti-estrogen EM-800 and tamoxifen on estrogen-sensitive parameters in intact mice. *Int J Cancer* **73**, 381-391 (1997).
24. L. Su, D. D. Mruk, C. Y. Cheng, Drug transporters, the blood-testis barrier, and spermatogenesis. *J Endocrinol* **208**, 207-223 (2011).
25. T. Abe, K. Sugimura, Y. Hosono, Y. Takami, M. Akita, A. Yoshimura, S. Tada, T. Nakayama, H. Murofushi, K. Okumura, S. Takeda, M. Horikoshi, M. Seki, T. Enomoto, The histone chaperone facilitates chromatin transcription (FACT) protein maintains normal replication fork rates. *J Biol Chem* **286**, 30504-30512 (2011).
26. L. Prendergast, E. Hong, A. Safina, D. Poe, G. K., Histone chaperone FACT is essential to overcome replication stress in mammalian cells. *Oncogene* **under revision** (2020).
27. B. C. Tan, C. T. Chien, S. Hirose, S. C. Lee, Functional cooperation between FACT and MCM helicase facilitates initiation of chromatin DNA replication. *EMBO J* **25**, 3975-3985 (2006).
28. J. Yang, X. Zhang, J. Feng, H. Leng, S. Li, J. Xiao, S. Liu, Z. Xu, J. Xu, D. Li, Z. Wang, J. Wang, Q. Li, The Histone Chaperone FACT Contributes to DNA Replication-Coupled Nucleosome Assembly. *Cell Rep* **14**, 1128-1141 (2016).
29. S. X. Zeng, Y. Li, Y. Jin, Q. Zhang, D. M. Keller, C. M. McQuaw, E. Barklis, S. Stone, M. Hoatlin, Y. Zhao, H. Lu, Structure-specific recognition protein 1 facilitates microtubule growth and bundling required for mitosis. *Mol Cell Biol* **30**, 935-947 (2010).
30. P. Immunological Genome, ImmGen at 15. *Nat Immunol* **21**, 700-703 (2020).
31. S. Gao, L. Yan, R. Wang, J. Li, J. Yong, X. Zhou, Y. Wei, X. Wu, X. Wang, X. Fan, J. Yan, X. Zhi, Y. Gao, H. Guo, X. Jin, W. Wang, Y. Mao, F. Wang, L. Wen, W. Fu, H. Ge, J. Qiao, F. Tang, Tracing the temporal-spatial transcriptome landscapes of the human fetal digestive tract using single-cell RNA-sequencing. *Nat Cell Biol* **20**, 721-734 (2018).
32. A. L. Haber, M. Biton, N. Rogel, R. H. Herbst, K. Shekhar, C. Smillie, G. Burgin, T. M. Delorey, M. R. Howitt, Y. Katz, I. Tirosh, S. Beyaz, D. Dionne, M. Zhang, R. Raychowdhury, W. S. Garrett, O. Rozenblatt-Rosen, H. N. Shi, O. Yilmaz, R. J. Xavier, A. Regev, A single-cell survey of the small intestinal epithelium. *Nature* **551**, 333-339 (2017).
33. R. G. Lindeboom, L. van Voorthuijsen, K. C. Oost, M. J. Rodriguez-Colman, M. V. Luna-Velez, C. Furlan, F. Baraille, P. W. Jansen, A. Ribeiro, B. M. Burgering, H. J. Snippert, M. Vermeulen, Integrative multi-omics analysis of intestinal organoid differentiation. *Mol Syst Biol* **14**, e8227 (2018).

34. G. Wittenburg, V. Flade, A. I. Garbe, G. Lauer, D. Labudde, Scaffold preferences of mesenchymal stromal cells and adipose-derived stem cells from green fluorescent protein transgenic mice influence the tissue engineering of bone. *Br J Oral Maxillofac Surg* **52**, 409-414 (2014).
35. M. F. Taha, V. Hedayati, Isolation, identification and multipotential differentiation of mouse adipose tissue-derived stem cells. *Tissue Cell* **42**, 211-216 (2010).
36. S. J. Huang, R. H. Fu, W. C. Shyu, S. P. Liu, G. P. Jong, Y. W. Chiu, H. S. Wu, Y. A. Tsou, C. W. Cheng, S. Z. Lin, Adipose-derived stem cells: isolation, characterization, and differentiation potential. *Cell Transplant* **22**, 701-709 (2013).
37. J. D. Buenrostro, P. G. Giresi, L. C. Zaba, H. Y. Chang, W. J. Greenleaf, Transposition of native chromatin for fast and sensitive epigenomic profiling of open chromatin, DNA-binding proteins and nucleosome position. *Nat Methods* **10**, 1213-1218 (2013).
38. R. K. Suto, R. S. Edayathumangalam, C. L. White, C. Melander, J. M. Gottesfeld, P. B. Dervan, K. Luger, Crystal structures of nucleosome core particles in complex with minor groove DNA-binding ligands. *J Mol Biol* **326**, 371-380 (2003).
39. D. J. Fitzgerald, J. N. Anderson, Selective nucleosome disruption by drugs that bind in the minor groove of DNA. *J Biol Chem* **274**, 27128-27138 (1999).
40. O. I. Kulaeva, F. K. Hsieh, V. M. Studitsky, RNA polymerase complexes cooperate to relieve the nucleosomal barrier and evict histones. *Proc Natl Acad Sci U S A* **107**, 11325-11330 (2010).
41. O. I. Kulaeva, D. A. Gaykalova, V. M. Studitsky, Transcription through chromatin by RNA polymerase II: histone displacement and exchange. *Mutat Res* **618**, 116-129 (2007).
42. M. A. Schwabish, K. Struhl, Evidence for eviction and rapid deposition of histones upon transcriptional elongation by RNA polymerase II. *Mol Cell Biol* **24**, 10111-10117 (2004).
43. G. Orphanides, G. LeRoy, C. H. Chang, D. S. Luse, D. Reinberg, FACT, a factor that facilitates transcript elongation through nucleosomes. *Cell* **92**, 105-116 (1998).
44. K. Gurova, H. W. Chang, M. E. Valieva, P. Sandlesh, V. M. Studitsky, Structure and function of the histone chaperone FACT - Resolving FACTual issues. *Biochim Biophys Acta Gene Regul Mech*, (2018).
45. S. Carvalho, A. C. Raposo, F. B. Martins, A. R. Grosso, S. C. Sridhara, J. Rino, M. Carmo-Fonseca, S. F. de Almeida, Histone methyltransferase SETD2 coordinates FACT recruitment with nucleosome dynamics during transcription. *Nucleic Acids Res* **41**, 2881-2893 (2013).
46. P. B. Mason, K. Struhl, The FACT complex travels with elongating RNA polymerase II and is important for the fidelity of transcriptional initiation in vivo. *Mol Cell Biol* **23**, 8323-8333 (2003).
47. J. D. True, J. J. Muldoon, M. N. Carver, K. Poorey, S. J. Shetty, S. Bekiranov, D. T. Auble, The Modifier of Transcription 1 (Mot1) ATPase and Spt16 Histone Chaperone Co-regulate Transcription through Preinitiation Complex Assembly and Nucleosome Organization. *J Biol Chem* **291**, 15307-15319 (2016).
48. E. Nesher, A. Safina, I. Aljahdali, S. Portwood, E. S. Wang, I. Koman, J. Wang, K. V. Gurova, Role of chromatin damage and chromatin trapping of FACT in mediating the anticancer cytotoxicity of DNA-binding small molecule drugs. *Cancer Res*, (2018).
49. F. K. Hsieh, O. I. Kulaeva, S. S. Patel, P. N. Dyer, K. Luger, D. Reinberg, V. M. Studitsky, Histone chaperone FACT action during transcription through chromatin by RNA polymerase II. *Proc Natl Acad Sci U S A* **110**, 7654-7659 (2013).
50. D. B. Stetson, R. Medzhitov, Type I interferons in host defense. *Immunity* **25**, 373-381 (2006).
51. K. Leonova, A. Safina, E. Nesher, P. Sandlesh, R. Pratt, C. Burkhart, B. Lipchick, I. Gitlin, C. Frangou, I. Koman, J. Wang, K. Kirsanov, M. G. Yakubovskaya, A. V. Gudkov, K. Gurova, TRAIN (Transcription of Repeats Activates INterferon) in response to chromatin destabilization induced by small molecules in mammalian cells. *Elife* **7**, (2018).

52. S. Parasuraman, R. Raveendran, R. Kesavan, Blood sample collection in small laboratory animals. *J Pharmacol Pharmacother* **1**, 87-93 (2010).
53. T. Sato, R. G. Vries, H. J. Snippert, M. van de Wetering, N. Barker, D. E. Stange, J. H. van Es, A. Abo, P. Kujala, P. J. Peters, H. Clevers, Single Lgr5 stem cells build crypt-villus structures in vitro without a mesenchymal niche. *Nature* **459**, 262-265 (2009).
54. A. Dobin, C. A. Davis, F. Schlesinger, J. Drenkow, C. Zaleski, S. Jha, P. Batut, M. Chaisson, T. R. Gingeras, STAR: ultrafast universal RNA-seq aligner. *Bioinformatics* **29**, 15-21 (2013).
55. M. I. Love, W. Huber, S. Anders, Moderated estimation of fold change and dispersion for RNA-seq data with DESeq2. *Genome Biol* **15**, 550 (2014).
56. U. Raudvere, L. Kolberg, I. Kuzmin, T. Arak, P. Adler, H. Peterson, J. Vilo, g:Profiler: a web server for functional enrichment analysis and conversions of gene lists (2019 update). *Nucleic Acids Res* **47**, W191-W198 (2019).
57. B. Langmead, S. L. Salzberg, Fast gapped-read alignment with Bowtie 2. *Nat Methods* **9**, 357-359 (2012).
58. F. Ramirez, F. Dundar, S. Diehl, B. A. Gruning, T. Manke, deepTools: a flexible platform for exploring deep-sequencing data. *Nucleic Acids Res* **42**, W187-191 (2014).
59. Y. Zhang, T. Liu, C. A. Meyer, J. Eeckhoute, D. S. Johnson, B. E. Bernstein, C. Nusbaum, R. M. Myers, M. Brown, W. Li, X. S. Liu, Model-based analysis of ChIP-Seq (MACS). *Genome Biol* **9**, R137 (2008).
60. G. Yu, L. G. Wang, Q. Y. He, ChIPseeker: an R/Bioconductor package for ChIP peak annotation, comparison and visualization. *Bioinformatics* **31**, 2382-2383 (2015).
61. T. Stuart, A. Butler, P. Hoffman, C. Hafemeister, E. Papalexi, W. M. Mauck, 3rd, Y. Hao, M. Stoeckius, P. Smibert, R. Satija, Comprehensive Integration of Single-Cell Data. *Cell* **177**, 1888-1902 e1821 (2019).
62. D. Aran, A. P. Looney, L. Liu, E. Wu, V. Fong, A. Hsu, S. Chak, R. P. Naikawadi, P. J. Wolters, A. R. Abate, A. J. Butte, M. Bhattacharya, Reference-based analysis of lung single-cell sequencing reveals a transitional profibrotic macrophage. *Nat Immunol* **20**, 163-172 (2019).

Acknowledgement: We are grateful for the help and support to the members of administrative office of Cell Stress Biology Department of Roswell Park Comprehensive Cancer Center, specifically to Mary Morgan, Sarah Tyrpak and Bruce Specht, to the members of shared resources facilities for the help and advise with the design and processing of experiments, specifically to Dr. Prashant Singh, director of Genomics shared facility, Dr. Joseph Spernyak, director of In vivo Imaging facility, Dr. Leslie Curtin, veterinarian, member of Department of Laboratory Animal Resources. This study was partially funded by NIH NCI grant R21CA198395 to KG, Roswell Park Alliance Foundation to KG and NCI NIH Core grant P30CA16056 to RPCCC.

Ssrp1$^{fl/fl}$ mice are available through MMRRC, ID:46323. NGD data are submitted to GEO Database. Submission numbers (pending). All other reagents and codes are available upon request.

Author contribution: IG performed part of animal experiments and most of cell-based experiments, drafted the manuscript. PS generated mouse model, characterized phenotype of mice upon FACT depletion and edited manuscript. AS generated genetically modified ESC and performed *in vitro* fertilization. IT is animal pathologist. MM and JW helped with bioininformatic

analyses, MM edited the manuscript. KG developed the concept of the study, analyzed all data, drafted, and edited the manuscript.

Authors declare no competing interests related to the reported study.

Figure Legends

Figure 1. Effect of *Ssrp1* KO in mice. A, B. Normalized weigh (A) and survival (B) of *Ssrp1*$^{fl/fl}$; *CreER*$^{T2+/+}$ mice of different age (in weeks) after start of tamoxifen (TMX) treatment. C. Normalized mean complete blood counts in *Ssrp1*$^{fl/fl}$; *CreER*$^{T2+/+}$ mice treated with vehicle or tamoxifen at day 7 after start of treatment (n = 3). * $p < 0.05$. D. Photographs of mice treated with vehicle or tamoxifen 7 days after start of treatment. E. Gross pathology examination of mouse euthanized due to 20% weight loss after treatment with tamoxifen and control vehicle treated mouse. Green and blue ovals indicate to subcutaneous and inguinal fat deposits respectively. F. MRI image of the same mouse before and after tamoxifen treatment.

Figure 2. Pathological finding in *Ssrp1*$^{fl/fl}$; *CreER*$^{T2+/+}$ mice at necropsy. A. H&E staining of section of mouse organs. B. Incidence of pathological findings. C. H&E stating of liver sections. Yellow arrow indicates to mitotic hepatocyte, blue arrows - to lymphocyte infiltration.

Figure 3. Depletion of FACT in mice leads to the reduced proliferation and death of cells in several organs. A, B. Effect of tamoxifen administration in *Ssrp1*$^{fl/fl}$; *CreER*$^{T2+/+}$ mice on replication in spleen (A) and intestine (B). EdU was given to mice 3 days after stop of tamoxifen treatment for 1 hour followed by organ isolation and staining for total DNA (Hoechst), EdU and SSRP1. C. Quantitation of EdU staining. D. Quantitation of IHC staining of tissue sections with antibody to cleaved caspase 3 (original data are shown on Fig.S7).

Figure 4. Effect of FACT depletion on cell composition of bone marrow of *Ssrp1*$^{fl/fl}$; *CreER*$^{T2+/+}$ mice (pooled data from 2 mice on day 1 after stop of treatment). A. UMAP plots with identified clusters shown in different colors. Blue dotted oval indicates clusters with significantly reduced number of cells, red – with significantly increased. Red arrow shows de novo emerged group of cells. B. UMAP plots colored according to cell type. C. Comparison of the number of cells identified in bone marrow of vehicle and tamoxifen treated animals. D. Fold change in the number of cells of different types upon FACT depletion. E. Venn diagram of marker genes of yellow and purple clusters of B cells. Number of common and specific cells are shown within circles. Significantly enriched gene set for yellow and purple clusters specific genes are shown on the left and right from the diagram and for common genes – below the diagram. Number in brackets is order of q-value of FDR. F. UMAP plot with four cell types colored. Areas of dashed squares are enlarged on panel G. G. Enlarged section of UMAP plot with stem cell clusters. H. Comparison of the number of stem cells identified in bone marrow of vehicle and tamoxifen treated animals. I. Summary of changes in the composition of stem cells in bone marrow upon FACT depletion. Dotted black circles show number of stem cells of each type in the presence of FACT, colored circles – number of cells upon FACT depletion, blue color emphasizes decrease and red increase in cell number. Arrows – directions of cell differentiation.

Figure 5. Effect of FACT depletion on cell composition of intestine of *Ssrp1*$^{fl/fl}$; *CreER*$^{T2+/+}$ mice (pooled data from 2 mice). A. UMAP plots with identified clusters shown in different colors. Blue dotted oval indicates clusters with significantly reduced number of cells, red – with significantly increased. B. Fold change in the number of cells of different types upon FACT depletion. Colors and numbers correspond to clusters shown on panel A. C. UMAP plot color-coded based on Lgr5 expression.

Figure 6. Depletion of FACT affects viability of stem, but not differentiated cells. A, B. Effect of 4-OHT administration on colony forming ability of bone marrow cells of different genotypes. *A*. Photographs of colonies of bone marrow cells kept in culture for 7 days in the presence or absence of 4-OHT. B. Quantitation of bone marrow colony assay. Bars – mean colony number per plate (n = 3). Error bars – SD. P values < 0.05 are shown. C, D. Growth of intestinal organoids in the presence or absence of 4-OHT. C. Photographs of small intestine organoids at different days after plating. D. Resorufin assay to assess cell viability of organoids in the presence and absence of 4-OHT. Bars - mean of two replicates, error bars – SD. P values below 0.05 are shown. E. Caspase activity in lysates of MSCs of different genotypes treated with vehicle or 4-OHT. Bars - mean of three replicates, error bars – SD. P values below 0.05 are shown. F, G. Effect of 4-OHT administration of intestinal organoids of different genotypes kept in the presence (undifferentiated conditions) or absence (differentiated conditions) of R-spondin 1. F. Bars - mean viability of two replicates of organoids assessed by resorufin assay, error bars – SD, p values below 0.05 are shown. G. IF staining of intestinal organoids from *Ssrp1*$^{fl/fl}$*; CreER*$^{T2+/+}$ mice kept in the presence or absence of R-spondin 1 with antibody to LGR5, SSRP1 and Hoechst (DNA). H-J. Effect of 4-OHT administration on MSC and their differentiated counterparts. H. Assessment of viability by methylene blue assay of MSC kept in conditions supporting their undifferentiated status, or their differentiation into osteocytes or adipocytes for 21 days and then treated with vehicle or 4-OHT. Bars – mean of 2 replicates. Error bars – SD. P values below 0.05 is shown. H. Staining of MSC, osteocytes and adipocytes with Alizarine Red (positive staining of osteocytes) or Oil Red (positive staining of adipocytes). J. Western blotting of protein extracts from MSCm adipocytes and osteocytes from mice of different genotype treated with vehicle or 4-OHT.

Figure 7. Comparison of RNA-seq data between MSC treated with vehicle or 4-OHT. A. Volcano plot of changes in transcript counts in 4-OHT treated cells versus control. Red dots indicate transcripts with absolute fold change $\geq$ 2 and FDR < 0.05. B. MA plot showing difference between changes in transcript counts in 4-OHT treated MSC vs control and average expression of the same transcript between conditions (baseMean). C, D. Dot plots with the results of GO enrichment for up (C) and down (D) regulated genes.

Figure 8. FACT depletion in MSC leads to the changes of chromatin accessibility in transcription dependent manner. A. Integrated genome browser view of normalized ATAC-seq read counts in control or 4-OHT treated MSC of different genotypes. Red arrows indicate peaks which were reduced, and horizontal brackets show areas where chromatin accessibility was increased in homozygous cells upon 4-OHT treatment. B. Quantitation of the number of peaks associated with different genomic features in MSC cells upon FACT loss. C. ATAC-seq read density profile and heatmap for fragments of all lengths showing mean read density over all mouse genes upon 4-OHT treatment. Red arrow indicates the difference in profiles at gene body. D. Examples of ATAC-seq read density profiles for nucleosome-free and mononucleosome fragments for genes expressed at different levels: left – top 1% genes, right bottom 25%. Profiles for all other transcription categories are shown on Fig. S12. F. Quantitation of mean read density at gene body (TSS – TES) for genes expressed at different levels. G. Example of mean read density profiles around TSS (+/- 1 kbp) for genes expressed at different levels: left – top 1% genes, right bottom 25%. Profiles for all other transcription categories are shown on Fig. S13. H. Comparison of Hoechst 33342 binding to leave to control and 4-OHT treated MSC cells of different genotypes.

Bars – median of fluorescent intensity. Error bar – SD. P value < 0.05 is shown. Histograms are shown on Fig.S14.

A

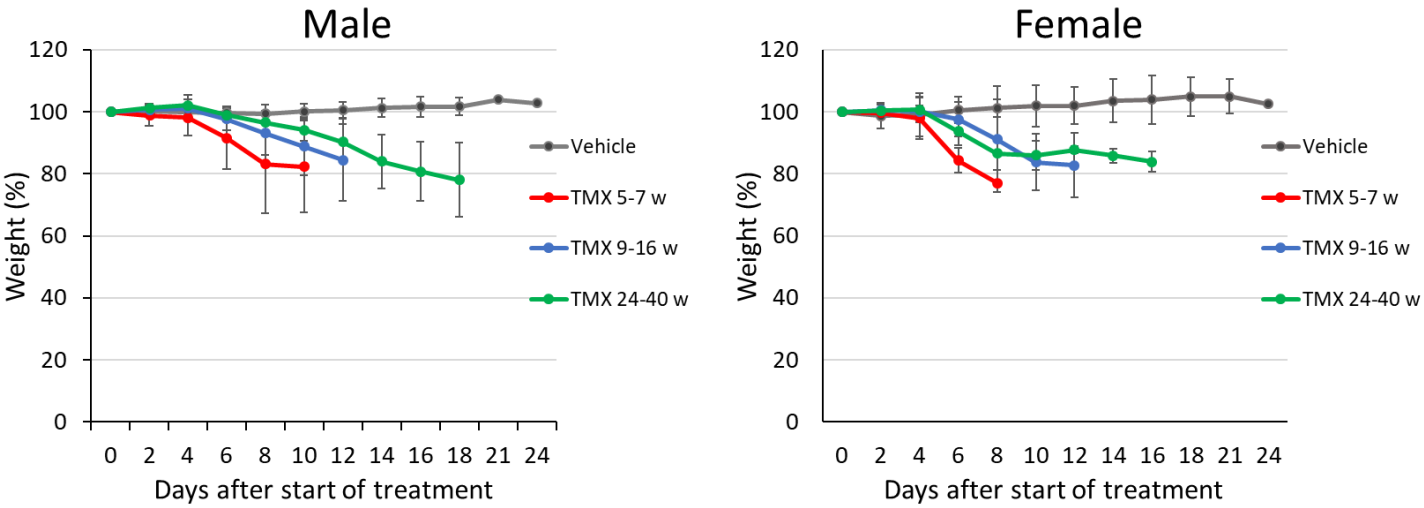

B

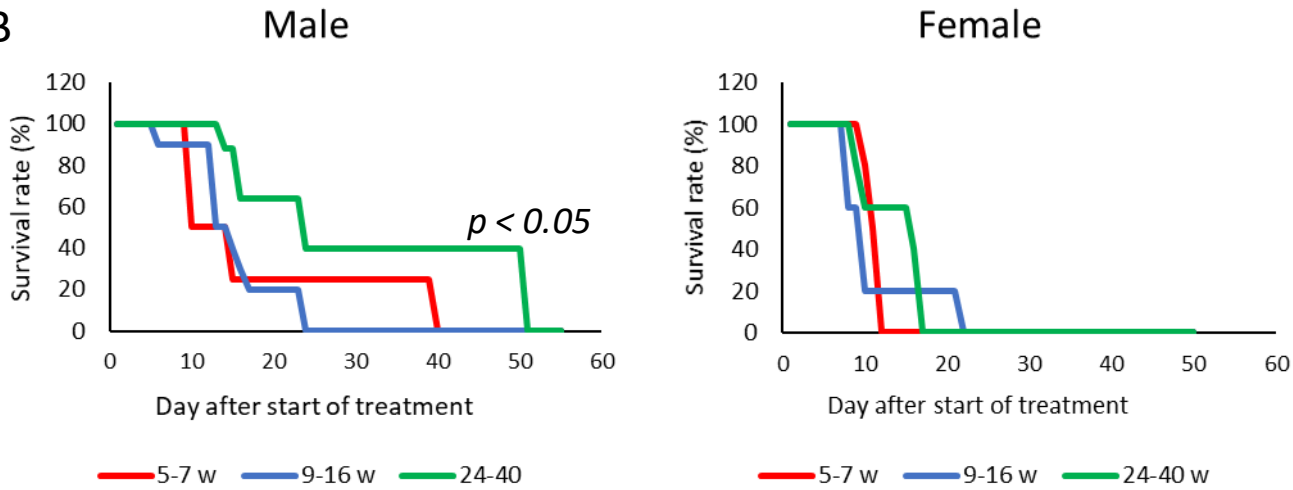

C

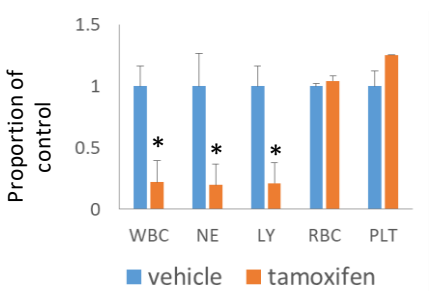

WBC – white blood cells
NE – neutrophils
LY –lymphocytes
RBC – red blood cells
PLT - platelets

D

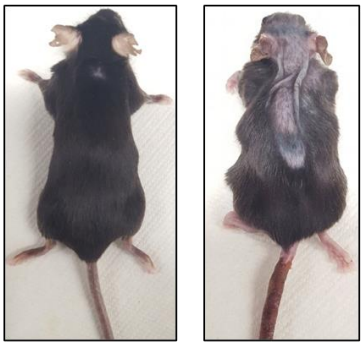

E

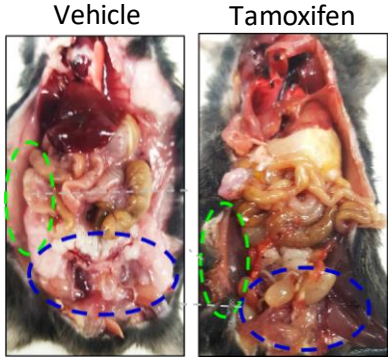

F

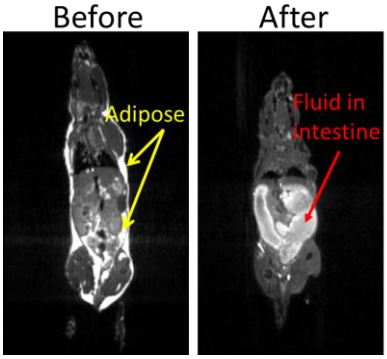

Figure 1

A

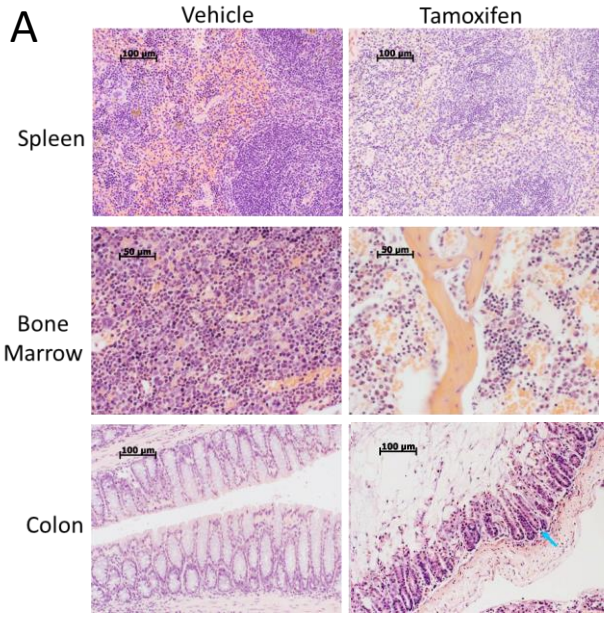

B

Organs	Vehicle		Tamoxifen	
	M (n=4)	**F** (n=2)	**M** (n=5)	**F** (n=4)
Liver	1/4	0/2	5/5	4/4
Lung	0/4	0/2	0/5	0/4
Bone Marrow	0/4	0/2	3/5	3/4
Spleen	0/4	0/2	2/5	3/4
Colon	0/4	0/2	2/5	2/5
Duodenum	0/4	0/2	1/5	1/4
Skin	0/4	0/2	4/5	0/4
Salivary Gland	0/4	0/2	3/5	0/4
Pancreas	0/4	0/2	2/5	0/4
Kidney	0/4	0/2	0/5	3/5

C

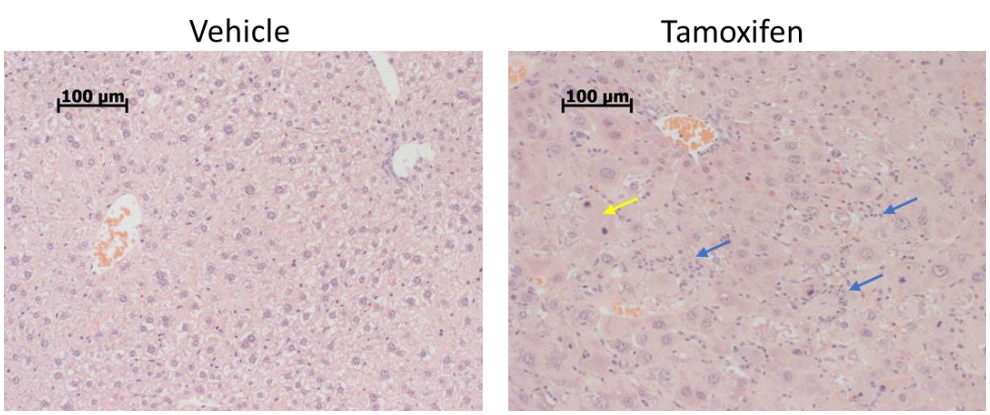

Figure 2

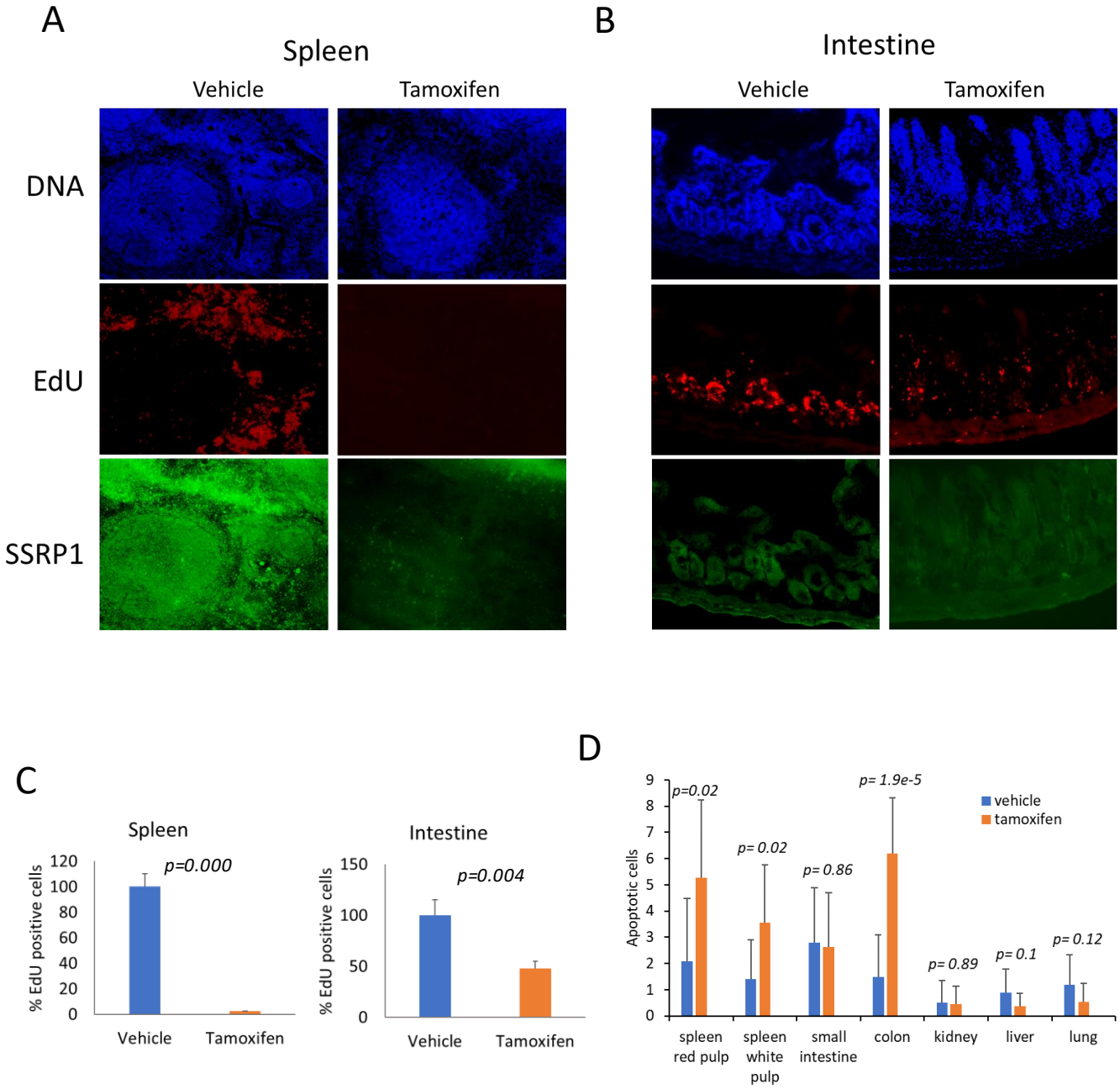
A
Spleen
Vehicle
Tamoxifen
DNA
EdU
SSRP1
B
Intestine
Vehicle
Tamoxifen
C
Spleen
% EdU positive cells
120
100
80
60
40
20
0
p=0.000
Vehicle
Tamoxifen
Intestine
% EdU positive cells
150
100
50
0
p=0.004
Vehicle
Tamoxifen
D
Apoptotic cells
9
8
7
6
5
4
3
2
1
0
p=0.02
p= 0.02
p= 0.86
p= 1.9e-5
p= 0.89
p= 0.1
p= 0.12
vehicle
tamoxifen
spleen red pulp
spleen white pulp
small intestine
colon
kidney
liver
lung

Figure 3

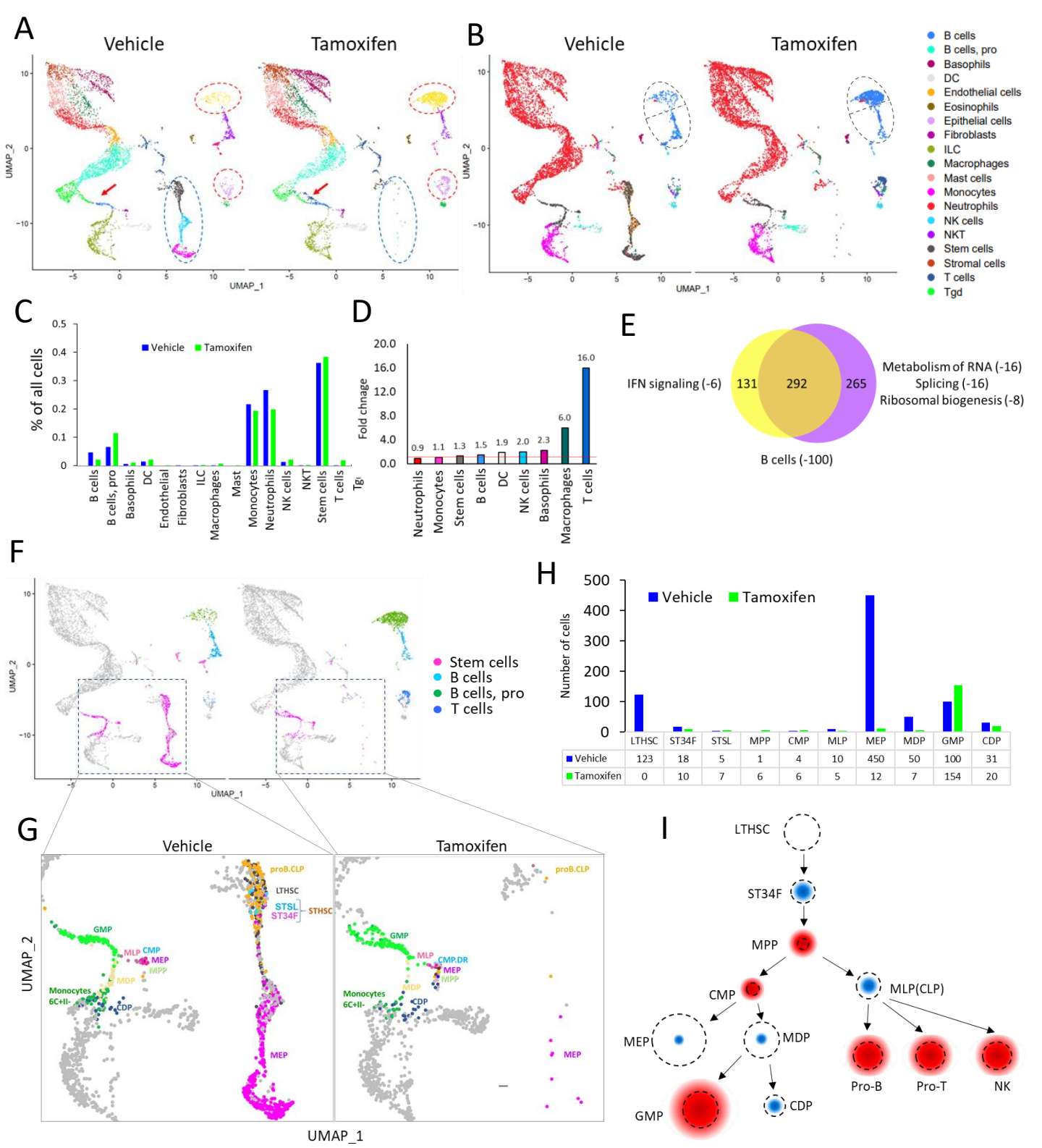
A
Vehicle
Tamoxifen
UMAP_2
UMAP_1
B
Vehicle
Tamoxifen
B cells
B cells, pro
Basophils
DC
Endothelial cells
Eosinophils
Epithelial cells
Fibroblasts
ILC
Macrophages
Mast cells
Monocytes
Neutrophils
NK cells
NKT
Stem cells
Stromal cells
T cells
Tgd
C
% of all cells
Vehicle
Tamoxifen
D
Fold chnage
0.9
1.1
1.3
1.5
1.9
2.0
2.3
6.0
16.0
Neutrophils
Monocytes
Stem cells
B cells
DC
NK cells
Basophils
Macrophages
T cells
E
IFN signaling (-6)
131
292
265
Metabolism of RNA (-16)
Splicing (-16)
Ribosomal biogenesis (-8)
B cells (-100)
F
Stem cells
B cells
B cells, pro
T cells
H
Number of cells
Vehicle
Tamoxifen
LTHSC ST34F STSL MPP CMP MLP MEP MDP GMP CDP
Vehicle 123 18 5 1 4 10 450 50 100 31
Tamoxifen 0 10 7 6 6 5 12 7 154 20
G
Vehicle
Tamoxifen
proB.CLP
LTHSC
STSL
ST34F
STHSC
GMP
MLP
CMP
MEP
MPP
MDP
Monocytes
6C+II-
CDP
CMP.DR
UMAP_2
UMAP_1
I
LTHSC
ST34F
MPP
CMP
MLP(CLP)
MEP
MDP
GMP
CDP
Pro-B
Pro-T
NK

Figure 4

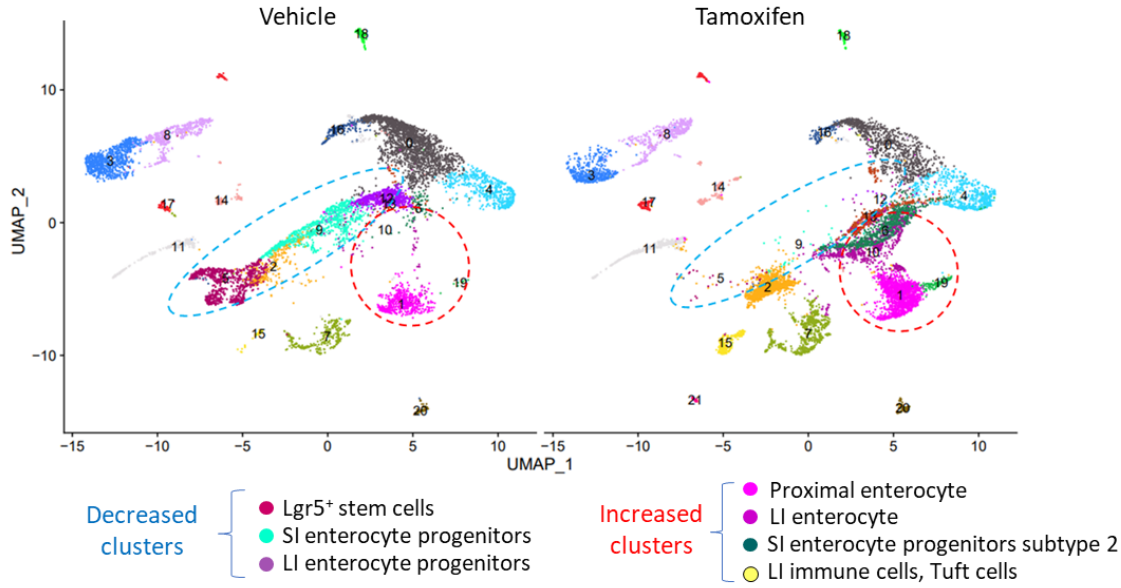
Vehicle
Tamoxifen
UMAP_2
UMAP_1
Decreased clusters
Lgr5⁺ stem cells
SI enterocyte progenitors
LI enterocyte progenitors
Increased clusters
Proximal enterocyte
LI enterocyte
SI enterocyte progenitors subtype 2
LI immune cells, Tuft cells

B

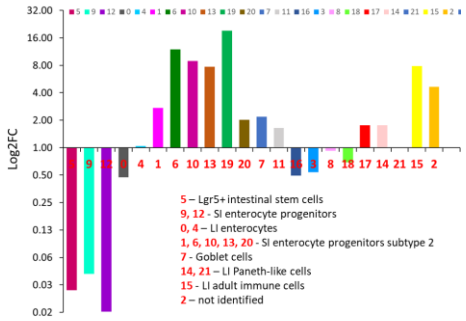
Log2FC
5 – Lgr5+ intestinal stem cells
9, 12 - SI enterocyte progenitors
0, 4 – LI enterocytes
1, 6, 10, 13, 20 - SI enterocyte progenitors subtype 2
7 - Goblet cells
14, 21 – LI Paneth-like cells
15 - LI adult immune cells
2 – not identified

C

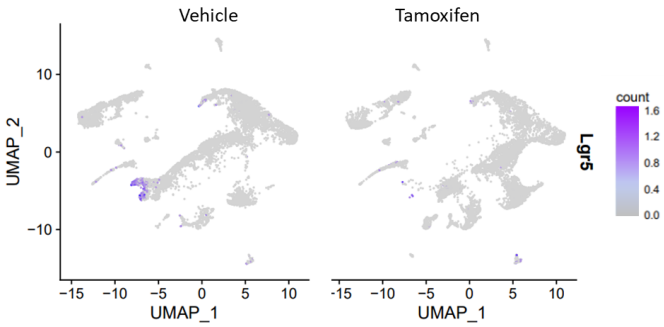
Vehicle
Tamoxifen
UMAP_2
UMAP_1
Lgr5
count

Figure 5

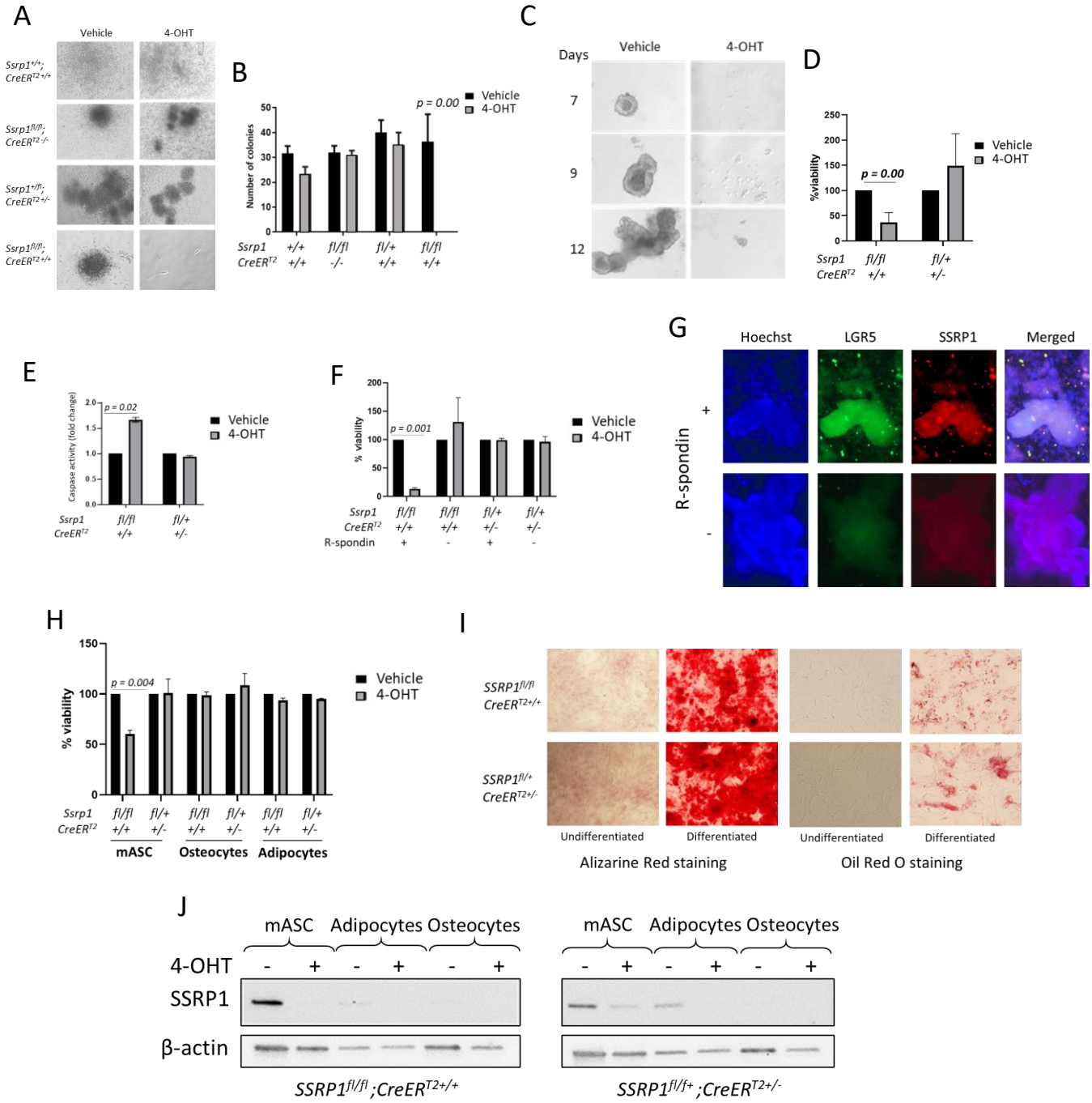
A
Vehicle
4-OHT
Ssrp1+/+; CreERT2+/+
Ssrp1fl/fl; CreERT2-/-
Ssrp1+/fl; CreERT2+/-
Ssrp1fl/fl; CreERT2+/+
B
p = 0.00
Vehicle
4-OHT
Number of colonies
Ssrp1 +/+ fl/fl fl/+ fl/fl
CreERT2 +/+ -/- +/+ +/+
C
Days
Vehicle
4-OHT
7
9
12
D
p = 0.00
Vehicle
4-OHT
%viability
Ssrp1 fl/fl fl/+
CreERT2 +/+ +/-
E
p = 0.02
Vehicle
4-OHT
Caspase activity (fold change)
Ssrp1 fl/fl fl/+
CreERT2 +/+ +/-
F
p = 0.001
Vehicle
4-OHT
% viability
Ssrp1 fl/fl fl/fl fl/+ fl/+
CreERT2 +/+ +/+ +/- +/-
R-spondin + - + -
G
Hoechst
LGR5
SSRP1
Merged
R-spondin
+
-
H
p = 0.004
Vehicle
4-OHT
% viability
Ssrp1 fl/fl fl/+ fl/fl fl/+ fl/fl fl/+
CreERT2 +/+ +/- +/+ +/- +/+ +/-
mASC
Osteocytes
Adipocytes
I
SSRP1fl/fl CreERT2+/+
SSRP1fl/+ CreERT2+/-
Undifferentiated
Differentiated
Undifferentiated
Differentiated
Alizarine Red staining
Oil Red O staining
J
mASC
Adipocytes
Osteocytes
4-OHT
- + - + - +
SSRP1
β-actin
SSRP1fl/fl ;CreERT2+/+
SSRP1fl/f+ ;CreERT2+/-

Figure 6

A

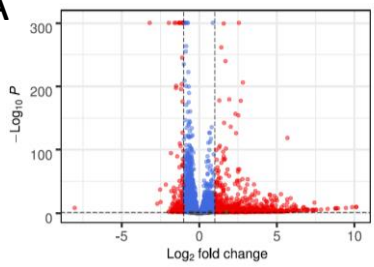

B

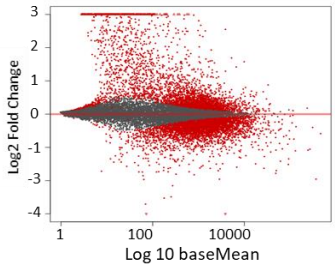

C

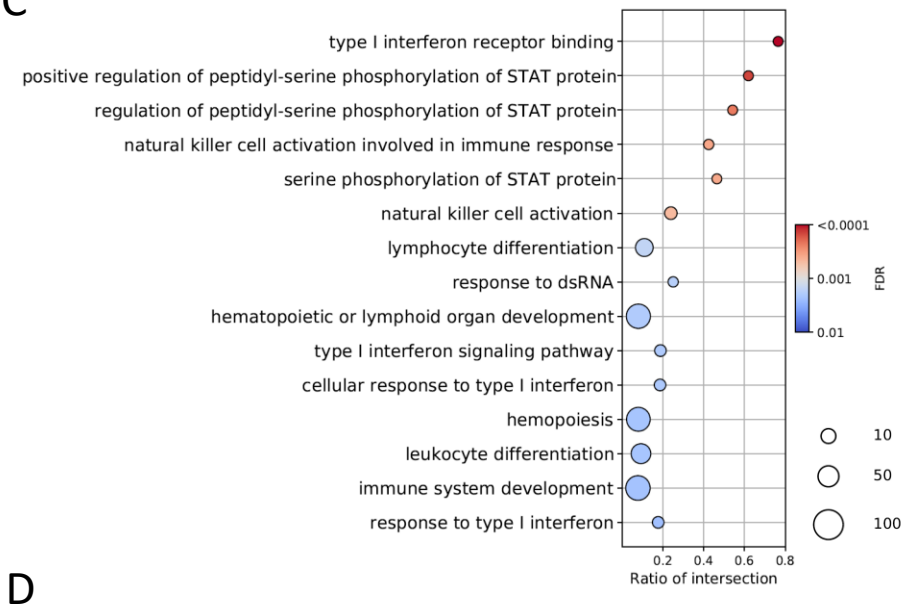

D

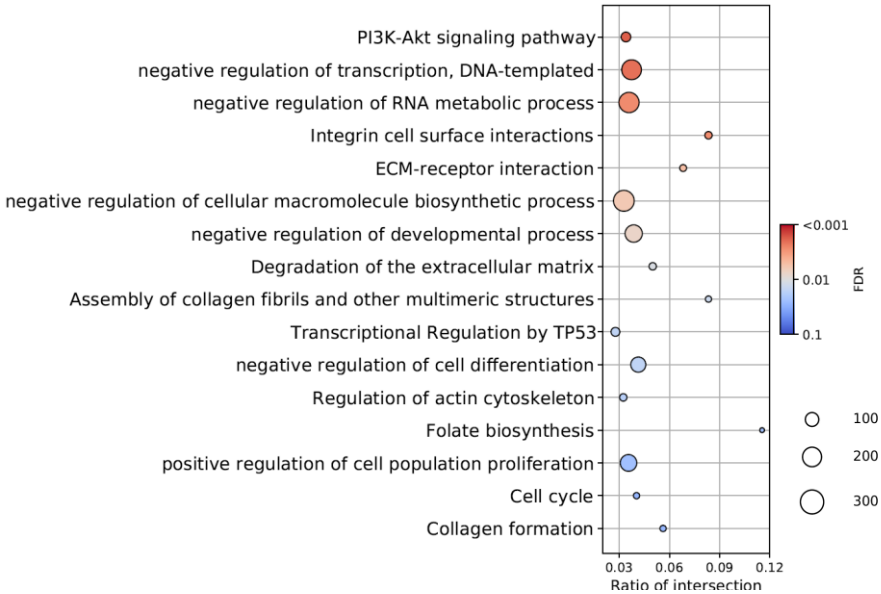

Figure 7

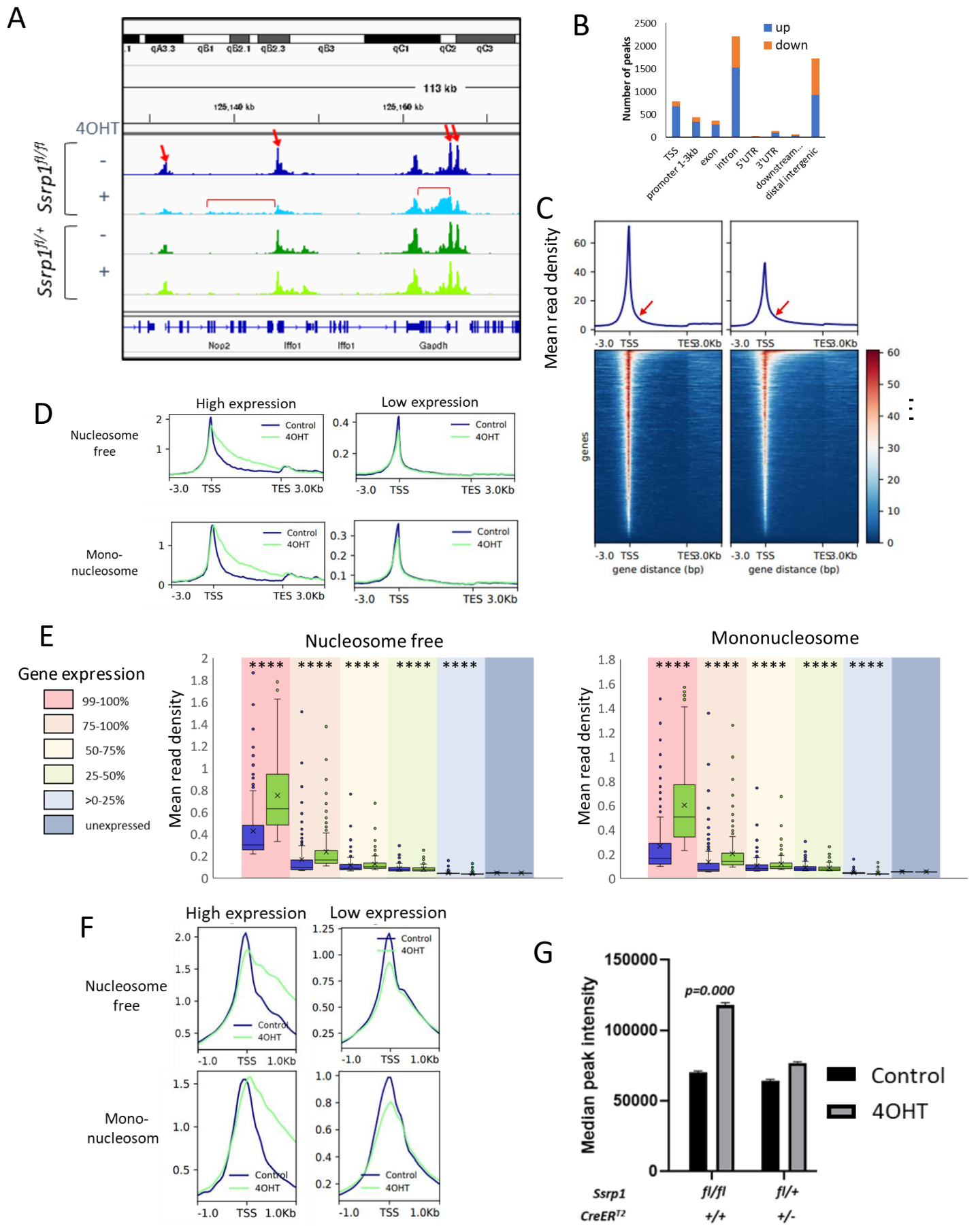
A
qA3.3
qB1
qB2.1
qB2.3
qB3
qC1
qC2
qC3
113 kb
125,140 kb
125,160 kb
4OHT
Ssrp1fl/fl
Ssrp1fl/+
-
+
Nop2
Iffo1
Iffo1
Gapdh
B
Number of peaks
up
down
TSS
promoter 1-3kb
exon
intron
5'UTR
3'UTR
downstream...
distal intergenic
C
Mean read density
-3.0 TSS TES3.0Kb
genes
gene distance (bp)
D
High expression
Low expression
Nucleosome free
Mono-nucleosome
Control
4OHT
-3.0 TSS TES 3.0Kb
E
Gene expression
99-100%
75-100%
50-75%
25-50%
>0-25%
unexpressed
Nucleosome free
Mononucleosome
Mean read density
****
F
High expression
Low expression
Nucleosome free
Mono-nucleosom
Control
4OHT
-1.0 TSS 1.0Kb
G
Median peak intensity
p=0.000
Control
4OHT
Ssrp1
CreERT2
fl/fl
+/+
fl/+
+/-

Figure 8